2014

Arabidopsis MSL10 Has a Regulated Cell Death Signaling Activity That Is Separable from Its Mechanosensitive Ion Channel Activity

Kira M. Veley
Washington University in St Louis

Grigory Maksaev
Washington University in St Louis

Elizabeth M. Frick
Washington University in St. Louis

Emma January
Washington University in St Louis

Sarah C. Kloepper
Washington University in St Louis

See next page for additional authors

Authors
Kira M. Veley, Grigory Maksaev, Elizabeth M. Frick, Emma January, Sarah C. Kloepper, and Elizabeth S. Haswell

Running title:

MS channel has two separable activities

Full title:

MSL10 has a regulated cell death signaling activity that is separable from its mechanosensitive ion channel activity

Kira M. Veley[1], Grigory Maksaev[1], Elizabeth M. Frick[1], Emma January[1], Sarah C. Kloepper[1], and Elizabeth S. Haswell[1]*

[1]Department of Biology, Box 1137
Washington University in St. Louis
Saint Louis, MO 63130

*Corresponding Author (ehaswell@wustl.edu)

Key words: Mechanosensitive, ion channel, MSL10, MscS, ROS, programmed cell death

Estimated length of manuscript: 15.0 pages

The author responsible for distribution of materials integral to the findings presented in this article in accordance with the policy described in the Instructions for Authors (www.plantcell.org) is: Elizabeth S. Haswell (ehaswell@wustl.edu).

ABSTRACT

Members of the MscS superfamily of mechanosensitive ion channels function as osmotic safety valves, releasing osmolytes under increased membrane tension. MscS homologs exhibit diverse topology and domain structure, and it has been proposed that the more complex members of the family might have novel regulatory mechanisms or molecular functions. Here we present a study of MscS-Like (MSL)10 from *Arabidopsis thaliana* that supports these ideas. High-level expression of MSL10-GFP in Arabidopsis induced small stature, hydrogen peroxide accumulation, ectopic cell death, and reactive oxygen species- and cell death-associated gene expression. Phosphomimetic mutations in the MSL10 N-terminal domain prevented these phenotypes. The phosphorylation state of MSL10 also regulated its ability to induce cell death when transiently expressed in *Nicotiana benthamiana* leaves, but did not affect subcellular localization, assembly or channel behavior. Finally, the N-terminal domain of MSL10 was sufficient to induce cell death in tobacco, independent of phosphorylation state. We conclude that the plant-specific N-terminal domain of MSL10 is capable of inducing cell death, this activity is regulated by phosphorylation, and MSL10 has two separable activities—one as an ion channel and one as an inducer of cell death. These findings further our understanding of the evolution and significance of mechanosensitive ion channels.

INTRODUCTION

How individual cells sense and respond to environmental stresses, and how they do so in the context of a multicellular organism, remain important biological problems. Much is unknown about the perception of stimuli that are mechanical in nature such as touch, gravity and membrane stretch (e.g., mechanotransduction), though it is clear that these types of signals are important regulators of growth and development in bacteria, plants and animals (Nakayama et al., 2012; Steffens et al., 2012; Lai et al., 2013; Mousavi et al., 2013; Yan et al., 2013). A particularly well-studied molecular mechanism for the perception and transduction of mechanical signals is provided by mechanosensitive (MS) ion channels, channels that open directly or indirectly in response to membrane tension (Arnadottir and Chalfie, 2010; Kung et al., 2010; Sukharev and Sachs, 2012). Genes that are predicted to encode MS channels are found in all three kingdoms of life, in a number of evolutionarily unrelated families (Liu et al., 2010; Nakayama et al., 2012; Sukharev and Sachs, 2012; Prole and Taylor, 2013).

The bacterial Mechanosensitive channel of Small conductance (MscS) from *Escherichia coli* is a leading model for the study of mechanosensation (Haswell et al., 2011; Martinac, 2011; Naismith and Booth, 2012). The four existing crystal structures of bacterial MscS (Bass et al., 2002; Steinbacher et al., 2007; Wang et al., 2008; Lai et al., 2013) reveal a channel comprising seven identical subunits. Each subunit contains three transmembrane (TM) helices, with the third TM helix of each monomer lining the pore. This pore extends into the vestibule of a large, cytoplasmic chamber that may serve to influence the composition of ions that pass through the channel (Gamini et al., 2011; Zhang et al., 2012; Cox et al., 2013). Along with several other MS ion channels in the bacterial membrane, MscS facilitates survival of hypoosmotic shock by releasing osmolytes when membrane tension increases beyond a certain threshold and is frequently referred to as an “osmotic safety valve” (Blount and Moe, 1999; Levina et al., 1999; Sotomayor et al., 2006; Boer et al., 2011; Reuter et al., 2014).

Homologs of MscS are found in nearly all bacterial species (Pivetti et al., 2003; Lai et al., 2013; Martinac et al., 2013), protozoa (Prole and Taylor, 2013), archaea (Palmieri et

76 al., 2009), some fungi (Nakayama et al., 2012), and all plant genomes so far analyzed
77 (Wilson et al., 2013), but have not been identified in animals. The region of sequence
78 similarity between MscS and other members of the MscS superfamily is restricted to a
79 relatively small portion of the protein that includes the pore-lining helix of MscS and
80 approximately 100 amino acids of the upper cytoplasmic domain (Kloda and Martinac,
81 2002; Pivetti et al., 2003; Balleza and Gomez-Lagunas, 2009; Haswell et al., 2011). *E.*
82 *coli* MscS is among the smallest members of its eponymous family of proteins, and
83 deletion studies indicate that it contains little non-essential protein sequence (Miller et
84 al., 2003b; Schumann et al., 2004). Other MscS family members, however, show
85 substantial variation in size and topology, containing anywhere from three to twelve TM
86 helices (Haswell et al., 2011) and a variety of domains not found in MscS, such as large
87 cytoplasmic loops, N- or C-terminal extensions, extracellular domains and ion or cyclic
88 nucleotide binding motifs (Li et al., 2002; Li et al., 2007; Haswell et al., 2011; Malcolm
89 and Maurer, 2012; Nakayama et al., 2012; Wilson et al., 2013).
90
91 The biological functions of few eukaryotic MSLs have been characterized to date, but it
92 appears that, like their bacterial homologs, they serve to respond to osmotic stresses.
93 MscS-Like (MSL)2 and MSL3 from *Arabidopsis thaliana* and MSC1 from the alga
94 *Chlamydomonas reinhardtii* are localized to the plastid or chloroplast envelope, where
95 they may provide a conduit for ions in response to osmotic imbalance between the
96 stroma and the cytoplasm (Haswell and Meyerowitz, 2006; Nakayama et al., 2007;
97 Veley et al., 2012). Msy1 and Msy2 from the fission yeast *Schizosaccharomyces pombe*
98 are localized to the endoplasmic reticulum (ER) where they regulate cytosolic Ca^{2+}
99 accumulation, also in response to osmotic shock (Nakayama et al., 2012). The function
100 of plasma membrane (PM)-localized MSLs remains under investigation. Arabidopsis
101 MSL10 is localized to the PM, and its MS ion channel properties have been
102 characterized in root protoplasts (Haswell et al., 2008) and Xenopus oocytes (Maksaev
103 and Haswell, 2012). However, *msl10* single mutants, *msl9 msl10* double mutants, and
104 even *msl4 msl5 msl6 msl9 msl10* quintuple mutant plants responded normally to a
105 number of mechanical and osmotic stresses (Haswell et al., 2008). Thus, it is quite
106 possible that MSLs from multicellular eukaryotes, while sensing the same stimulus as

107 MscS, respond to membrane tension in a different way or in a different physiological
108 context.
109
110 As a result, we and others have previously speculated that the topological and domain
111 diversity associated with MscS homologs indicates a multiplicity of functions and
112 regulatory mechanisms, and further proposed that MscS homologs might serve as
113 membrane tension sensors with outputs independent of ion flux (Haswell et al., 2011;
114 Wilson et al., 2013; Cox et al., 2014). Here we present a structural and functional
115 analysis of Arabidopsis MSL10 that supports these ideas. The plant-specific N-terminal
116 domain of MSL10 was capable of inducing hydrogen peroxide accumulation, ectopic
117 cell death, and the induction of reactive oxygen species- and cell death-associated
118 genes. This activity could be physically and genetically separated from the role of
119 MSL10 as an ion channel and was regulated by the phosphorylation state of specific
120 residues within the N-terminal domain. This work provides strong evidence for the
121 functional regulation of a MscS family member by posttranslational modification of an
122 organism-specific sequence and opens up the possibility that MSL10 has multiple
123 membrane tension-regulated activities. Ultimately, these findings are important for
124 furthering our understanding of the evolution and biological significance of
125 mechanosensitive channels in eukaryotes.
126
127 **RESULTS**
128
129 **Overexpression of MSL10-GFP results in small stature, hydrogen peroxide**
130 **accumulation, ectopic cell death, and the transcriptional activation of reactive**
131 **oxygen species- and cell death-associated genes.** We generated stably transformed
132 Arabidopsis homozygous lines in the Columbia ecotype (Col-0, referred to here as WT)
133 overexpressing *MSL10* cDNA from the constitutive and strong Cauliflower Mosaic Virus
134 *35S* promoter (*P35S*) (Odell et al., 1985; Jefferson et al., 1987). GFP was fused to the
135 C-terminus of MSL10; this tag has no effect on the channel properties of MSL10 when
136 expressed in Xenopus oocytes (Maksaev and Haswell, 2012) or root protoplasts
137 (Haswell et al., 2008). We observed that MSL10-GFP overexpression lines exhibited a

138 range of phenotypes, including dwarfism and brown patches on the leaf margins (Figure
139 1A, top row). Similar phenotypes were observed in plants grown under short-day
140 conditions (8 hours of light, Supplemental Figure 1A online), indicating that they are not
141 the result of a stressful light regime. We selected three T2 lines with a range of
142 phenotypic severity for further analysis. Elevated *MSL10-GFP* expression in these lines
143 was confirmed by reverse transcription PCR (RT-PCR) (Figure 1B).
144
145 The brown patches on the leaves of plants overexpressing *MSL10-GFP* resembled
146 lesions resulting from the activation of programmed cell death (PCD), a highly regulated
147 process that is initiated during senescence or immune response (Gan and Amasino,
148 1997; Diaz et al., 2006; Kotchoni and Gachomo, 2006; Gill and Tuteja, 2010). One
149 hallmark of PCD is the production of reactive oxygen species (ROS) like hydrogen
150 peroxide (H_2O_2), which are used as both a signal for and a facilitator of stress and PCD-
151 associated pathways (Desikan et al., 1998; Mittler et al., 2004; Cui et al., 2013). We
152 therefore stained leaf number 4 or 5 from 2-week-old WT plants or MSL10-GFP
153 overexpression lines with 3,3'-Diaminobenzidine (DAB) or trypan blue (Figure 1A,
154 middle and bottom row). We observed that all three overexpression lines stained with
155 DAB had increased levels of a dark brown precipitate compared to WT, indicative of the
156 increased presence of H_2O_2. Additionally, the two lines that appeared to have the
157 highest levels of H_2O_2 production, 12-3 and 15-2, also stained with trypan blue, a
158 commonly used indicator of lesion development, at three weeks of age. Trypan blue
159 staining was not detected in leaves from WT or line 7-1 (Figure 1A). The observed
160 levels of H_2O_2 accumulation and lesion formation roughly correlated with the amount of
161 *MSL10* overexpression; line 12-3 was the most severe and line 7-1 had a milder
162 phenotype (Figures 1A, B). Thus, overexpression of *MSL10-GFP* resulted in the
163 accumulation of H_2O_2 in leaf cells and patches of ectopic cell death.
164
165 After three weeks of growth, overexpression lines had acquired significantly less mass
166 (mg per rosette), weighing four to ten times less than the untransformed WT control
167 (Figure 1C). The average leaf epidermal pavement cell area in each line was calculated
168 from confocal laser scanning microscopy (CLSM) images of the adaxial surfaces of

169 rosette leaves stained with propidium iodide (PI) to highlight the plasma membrane.
170 Examples of the images used for this analysis are shown in Figure 1D. We found that
171 the average area of an adaxial pavement cell in the overexpression lines was less than
172 half that of WT (Figure 1D). Thus the *MSL10-GFP* overexpression lines may be smaller
173 due to reduced cell expansion.
174
175 To determine which cell death pathways might be induced in response to *MSL10-GFP*
176 overexpression, we compared the expression levels of genes involved in a range of cell
177 death- and ROS-associated pathways between WT and *MSL10-GFP* overexpressing
178 plants. We selected for analysis five genes reported to be induced by either biotic or
179 abiotic stress and involved in ROS production, PCD, or senescence. *SAG12* encodes a
180 cysteine protease and is a well-established transcriptional marker of senescence (Gan
181 and Amasino, 1997; Fischer-Kilbienski et al., 2010; Brusslan et al., 2012; Koyama et al.,
182 2013), *OSM34* encodes an osmotin-like protein (Capelli et al., 1997; Abdin et al., 2011;
183 Sharma et al., 2013) and *DOX1* encodes an alpha-dioxygenase that protects plant cells
184 from oxidative stress and plays an important role in mediating pathogen-induced cell
185 death (De Leon et al., 2002; Blanco et al., 2005). Additionally, *PERX34* encodes a
186 peroxidase that promotes H_2O_2 production in response to biotic stresses (Bindschedler
187 et al., 2006; Daudi et al., 2012) and *KTI1* encodes a trypsin inhibitor that modulates
188 PCD (Li et al., 2008). RT-PCR was performed on cDNA synthesized from RNA
189 extracted from 3-week-old whole rosette tissue. As expected, all five genes were
190 expressed at low to undetectable levels in healthy WT plants. However, all of the genes
191 tested were the most highly expressed in line 12-3, which also had the highest level of
192 *MSL10-GFP* transcript (Figure 1B) and MSL10 protein (Figure 1E) production, the
193 darkest DAB staining, and the most striking lesion formation (Figure 1A). While the 7-1
194 line showed intermediate levels of *MSL10* transcript and an intermediate reduction in
195 rosette size, it exhibited low DAB and trypan blue staining, and *SAG12, OSM34, and*
196 *DOX1* transcripts were not detected (Figure 1). These observations are consistent with
197 recent evidence that many measures of abiotic stress do not respond linearly to stress
198 level, and that shoot growth is often the most sensitive parameter (Claeys et al., 2014).
199 These data indicate that a number of biotic and abiotic stress pathways are activated at

200 the transcriptional level by high levels of *MSL10-GFP*. Taken together, the data
201 presented in Figure 1 show that ectopic overexpression of MSL10 promotes cell death
202 and ROS accumulation in stably transformed Arabidopsis lines.
203
204 **The MSL10 N-terminal domain is phosphorylated *in vivo* and is specific to**
205 **plants.** At least nine independent high-throughput proteomic analyses of
206 phosphorylated proteins have identified phosphorylated residues in peptides derived
207 from the N-terminal region of MSL10, which is predicted to be soluble and cytoplasmic
208 (aa 1-164, Figure 2). MSL10 S29, S46, S48, S57, S128, S131, and T136 are *in vivo*
209 phosphorylated in suspension cells (Nühse et al., 2004; Benschop et al., 2007;
210 Sugiyama et al., 2008; Li et al., 2009; Nakagami et al., 2010), seedlings (Engelsberger
211 and Schulze, 2012; Wang et al., 2013) and adult plants (Reiland et al., 2009; Reiland et
212 al., 2011). These data are summarized in Figure 2 and in Supplemental Table 1 online,
213 and can also be accessed via the PhosPhAt 4.0 database (http://phosphat.mpimp-
214 golm.mpg.de). The soluble N-terminal domain of MSL10 is specific to MSL10 and its
215 orthologs in other plants (Supplemental Figure 2 online) and does not share homology
216 with any region in MscS (Supplemental Figure 3 online). Indeed, this region does not
217 contain any identified conserved functional domains and shows the least sequence
218 homology among the Class II MSLs from Arabidopsis (49% amino acid sequence
219 identity, compared to 68% in the rest of the protein). We therefore sought to determine if
220 this MS10-specific sequence plays an important functional role and if such a function
221 might be regulated by phosphorylation.
222
223 **Phosphomimetic mutations in the MSL10 N-terminal domain prevent the**
224 **phenotypes caused by overexpression of wild-type MSL10-GFP.** In order to
225 investigate potential regulatory roles for the phosphorylation state of the MSL10 N-
226 terminal domain, we made a series of point mutations at the four residues identified as
227 phosphorylated under the greatest range of conditions (S57, S128, S131, and T136,
228 Supplemental Table 1 online). We introduced genetic lesions that mimicked either the
229 phosphorylated or the unphosphorylated state, a well-established technique used to
230 study the functional relevance of potential phosphorylation sites (Kaufman et al., 1989;

231 Cui et al., 2004; Qiao et al., 2012). These four residues were changed to either
232 aspartate or glutamate in order to mimic constitutive phosphorylation depending on
233 which was most convenient given the wild-type mRNA sequence (MSL10 S57D,
234 S128D, S131E, and T136D is designated MSL10^{4D} here for simplicity), or to alanine to
235 prevent phosphorylation (designated MSL10^{4A}). Overexpression of *MSL10^{4D}-GFP*
236 caused none of the phenotypes observed in the wild-type *MSL10-GFP* overexpression
237 lines, including H_2O_2 production (Figure 1A middle row), cell death (Figure 1A bottom
238 row), plant size (Figure 1A top row, 1C), or cell expansion (Figure 1D), despite having
239 high levels of *MSL10-GFP* mRNA (Figure 1B) and MSL10 protein (Figure 1E).
240 Overexpression of *MSL10-GFP^{4D}* did not activate *SAG12*, *OSM34*, *DOX1*, or *PERX34*
241 and resulted in only slightly increased transcriptional activation of *KTI1* (Figure 1B).
242 *PERX34* levels were also elevated in 5-day-old seedlings overexpressing wild-type
243 MSL10-GFP compared to the WT, but not in seedlings overexpressing MSL10-GFP^{4D}.
244 *SAG12*, *OSM34*, *DOX1*, and *KTI1* did not exhibit this pattern in seedlings
245 (Supplemental Figure 1B online). We were unable to isolate plants expressing
246 detectable levels of MSL10^{4A}-GFP (approximately 200 T_1 individuals were analyzed by
247 CLSM), which will be discussed further below. These data indicate that the identities of
248 the residues S57, S128, S131, and T136 were critical for the observed MSL10
249 overexpression phenotypes and that the phosphorylation status of these residues may
250 be a vital component of MSL10 function.
251
252 **The phosphorylation state of the MSL10 N-terminal domain regulates its**
253 **ability to induce cell death in a transient expression system.** Because we were
254 unable to isolate stably transformed Arabidopsis overexpressing MSL10^{4A}-GFP, and to
255 provide further support for MSL10 as an inducer of cell death, we employed a transient
256 expression system to more systematically investigate the effect of phosphorylation on
257 MSL10 function and to quantitatively assess cell death. We therefore used transient
258 overexpression of MSL10 variants in *Nicotiana benthamiana* (tobacco) leaves to
259 analyze the effect that the number of phosphorylated residues had on MSL10 activity by
260 expressing MSL10 with two (S128, S131), four (S57, S128, S131, T136), or seven
261 (S29, S46, S48, S57, S128, S131, T136) phosphorylated residues mutated. Wild-type

262 (*P35S:MSL10-GFP*), phosphomimetic (*P35S:MSL10^{D}-GFP*), or alanine-substitution
263 (*P35S:MSL10^{A}-GFP*) versions of MSL10 were transiently overexpressed in tobacco
264 leaves via infiltration with *Agrobacterium tumefaciens* transformed with the binary vector
265 pK7FWG2 (Karimi et al., 2002) harboring the appropriate MSL10 sequences. A plasmid
266 encoding the *p19* gene of tomato bushy stunt virus, which is often used in transient
267 expression systems to inhibit transgene silencing (Voinnet et al., 2003; Waadt and
268 Kudla, 2008; Garabagi et al., 2012), was co-infiltrated with each construct. Three days
269 after infiltration, successful expression was confirmed through GFP fluorescence
270 (Figure 3A, top row). By 5 days post-infiltration, GFP signal had disappeared in some
271 cells of the leaves expressing *P35S:MSL10-GFP* and *P35S:MSL10^{A}-GFP* (Figure 3A,
272 second row), and trypan blue staining indicated the appearance of patches of dead cells
273 in leaves expressing these constructs (Figure 3A, third row). In order to quantify this
274 effect at the cellular level, the percentage (averaged over 3 different infiltration
275 experiments) of dead epidermal pavement cells from the abaxial surface of leaves
276 expressing MSL10-GFP variants was determined by PI and fluorescein diacetate (FDA)
277 viability staining (Chaves et al., 2002). Vacuolar integrity was also used as an indication
278 of vitality and was assessed using a combination of false DIC (pseudocolored gray) and
279 localization of FDA. Representative images of cells classified as dead or alive using this
280 method are presented in Figure 3A, bottom row, and additional examples of raw data
281 used in the analysis, along with further information about the assay can be found in
282 Supplemental Figure 4 online. Statistical differences between these samples were
283 analyzed by one-way ANOVA and Tukey's test, and the "a" and "b" classes indicated in
284 Figure 3B represent significant differences with $p < 0.05$.
285
286 Consistent with what we observed in stably transformed Arabidopsis lines, we
287 found that expression of wild-type MSL10-GFP resulted in the death of approximately
288 25% of tobacco epidermal pavement cells, while expression of *p19* alone resulted in the
289 death of just 5% of the cells 5 days after infiltration (Figure 3B). Furthermore, replacing
290 the residues known to be phosphorylated *in vivo* with phosphomimetic amino acids
291 completely ameliorated MSL10-induced cell death. Infiltration with MSL10^{4D}-GFP and
292 MSL10^{7D}-GFP resulted in levels of cell death that were statistically inseparable from that

293 observed with the *p19* only control, causing approximately 9% and 7% cell death,
294 respectively (Figure 3A right panel, Figure 3B group "b"). Additionally, expressing
295 $MSL10^{2D}$-GFP caused 14% of cells to die, a value which could not be statistically
296 separated from either group "a" or "b" (2, Figure 3B), suggesting a threshold effect with
297 respect to the number of residues altered to mimic phosphorylation.
298
299 On the other hand, replacing two, four, or all seven of the *in vivo* phosphorylated
300 residues with alanine resulted in increased levels of cell death, with 20%, 29% and 35%
301 cell death observed, respectively. These samples were statistically inseparable from
302 each other and from cells infiltrated with the wild-type MSL10-GFP (Figure 3B, group a,
303 Figure 3A, left panel). All MSL10 variants tested produced similar GFP signal and
304 transformation efficiency at 3 days post-infiltration (Figure 3A, top row) and similar
305 protein levels in whole tobacco leaf extracts at 5 days post-infiltration (Figure 3C).
306 Taken together, these data demonstrate that the phosphorylation state of the MSL10 N-
307 terminal domain regulates its ability to promote cell death when overexpressed in plant
308 cells. A likely explanation for the observation that ectopic overexpression of wild-type
309 MSL10-GFP resulted in high levels of cell death in either stably transformed Arabidopsis
310 (Figure 1) or transiently-expressing tobacco epidermal cells (Figure 3) is that the cell
311 cannot maintain all copies of MSL10 in the phosphorylated state when it is expressed at
312 high levels and that the resulting subpopulation of unphosphorylated MSL10 is capable
313 of inducing cell death. The phosphorylated form of MSL10, the inactive form of the
314 protein with respect to inducing cell death, is thus likely to be the default state of MSL10
315 *in vivo,* consistent with the fact that at least nine phosphoproteomic studies on a variety
316 of tissue types under a multitude of conditions all identify the MSL10 N-terminal domain
317 as phosphorylated (Supplemental Table 1 online).
318
319 **Preventing or mimicking phosphorylation of the MSL10 N-terminal domain**
320 **does not demonstrably affect subcellular localization, assembly, or**
321 **electrophysiological properties of the channel.** In order to better understand the
322 molecular basis for these results, we tested the effects of the same point mutations on
323 three characteristics of the MSL10 protein: subcellular localization, interaction between

324 monomers and electrophysiological properties. It is well established that the
325 phosphorylation state of ion channels can affect their trafficking and localization (Maurel
326 et al., 2009; Bayle et al., 2011; Rice et al., 2012), so we tested whether phosphorylation
327 altered the subcellular localization of MSL10-GFP variants when transiently
328 overexpressed in tobacco. We transiently co-expressed MSL10 variants and organelle-
329 specific markers fused to mCherry (Nelson et al., 2007) and looked for co-localization
330 using CLSM. As previously shown with stably-transformed Arabidopsis expressing
331 MSL10-GFP under the control of its own promoter (Haswell et al., 2008), wild-type
332 MSL10-GFP exhibited localization to both the ER and the PM (Figure 4A, second
333 column). The subcellular localizations of $MSL10^{4D}$-GFP and $MSL10^{4A}$-GFP were
334 indistinguishable from each other and from wild-type MSL10-GFP (Figure 4A, third and
335 right-most columns). In addition, MSL10-GFP, $MSL10^{4A}$-GFP, and $MSL10^{4D}$-GFP were
336 found in the Hechtian strands of plasmolysed tobacco leaf cells (Figure 4A, bottom row).
337 In conclusion, all MSL10 variants showed similar localization patterns, though it remains
338 possible that the proportion of protein at a given subcellular location could differ
339 between the wild type and phospho-mutant forms.
340
341 Phosphorylation state is also known to play an important regulatory role in protein-
342 protein interactions (Marin et al., 2012; Orr, 2012; Ebert et al., 2013). *E. coli* MscS forms
343 a homo-heptameric channel (Bass et al., 2002; Miller et al., 2003a), and MSL10 is likely
344 to form a multimer as well. We tested for interactions among MSL10 variants using the
345 mating-based split-ubiquitin yeast two-hybrid assay, which is specifically designed to
346 detect interactions between membrane-localized proteins (Ludewig et al., 2003; Obrdlik
347 et al., 2004). As expected, we found that wild-type MSL10 was capable of self-
348 interaction and also observed that MSL10 could interact with $MSL10^{7A}$ or $MSL10^{7D}$ in a
349 yeast growth assay (Figure 4B, top row and left column). Furthermore, $MSL10^{7A}$ and
350 $MSL10^{7D}$ mutant forms were able to interact efficiently with themselves (Figure 4B,
351 second and third rows and columns). None of the variants tested showed evidence of
352 auto-activating the reporter (Figure 4B, empty NubG column). These data indicate that
353 MSL10 monomer-monomer interactions in the yeast two-hybrid assay were unaffected
354 by either type of lesion at phosphorylated residues.

355

356 A third potential role for phosphorylation of the MSL10 N-terminal domain is in the
357 regulation of its ion channel properties, as has been shown for TPK1 (Latz et al., 2007),
358 TRP (Voolstra et al., 2010), CLH-3b (Yamada et al., 2013) and PIP2 (Prado et al.,
359 2013). Mutations outside the membrane-spanning pore of bacterial MscS homologs
360 alter channel conductance (Zhang et al., 2012; Cox et al., 2013) and gating properties
361 (Nomura et al., 2008; Vasquez et al., 2008; Belyy et al., 2010; Koprowski et al., 2011). If
362 the MSL10 N-terminal domain interacts with the rest of the channel, the mutation of
363 seven charged amino acids could alter channel properties. As we previously
364 characterized MSL10 expressed heterologously in Xenopus oocytes by single channel
365 patch clamp electrophysiology (Maksaev and Haswell, 2012), we used this same assay
366 here to test the effect of phosphomimetic and alanine-substitution mutations on the
367 mechanosensitive gating and conductance properties of MSL10. All MSL10 variants,
368 regardless of phosphorylation state, were well expressed in Xenopus oocytes
369 (Supplemental Figure 5 online). Strong fluorescent signal (GFP for wild type, YFP for
370 phospho-mutants) was detected at the oocyte periphery, typically starting from 48-72
371 hours after injection (Supplemental Figure 5 online), consistent with our observation in
372 plant cells that MSL10 variants do not differ in subcellular localization (Figure 4A).

373

374 We chose 7 days post-injection for analysis because this produced the optimal number
375 of active channels per patch. Electrophysiological analysis of inside out excised
376 membrane patches pulled from oocytes expressing MSL10 variants revealed the
377 presence of tension-activated channels. The representative traces shown in Figure 4C
378 illustrate that all MSL10 variants exhibited hysteresis, a hallmark of MSL10 activity,
379 wherein the channel closes at a much lower pressure than at which it opens (Figure 4C,
380 Supplemental Figure 5 online.) Furthermore, we did not observe any differences in
381 tendency to flicker or in the average number of active channels in each patch between
382 the variants. Finally, though the variability in these measurements was high (the
383 membrane tension in a membrane patch produced by a given amount of pressure can
384 vary widely due to differences in patch size and geometry (Suchyna et al., 2009)), all
385 three MSL10 variants had similar threshold tensions for opening and similar ratios of

386 opening to closing tensions (Supplemental Figure 5 online). Current/voltage (I/V) curves
387 measured for single-channel openings between -50 mV and +50 mV were identical for
388 MSL10-GFP, MSL10^{4A}-YFP, MSL10^{7A}-YFP, MSL10^{4D}-YFP, and MSL10^{7D}-YFP (Figures
389 4D and Supplemental Figure 5 online). Taken together, the data shown in Figure 4
390 establish that the phosphorylation state of the MSL10 N-terminal domain does not
391 appreciably govern the subcellular localization, oligomerization, or channel properties of
392 MSL10.
393
394 **The MscS homology domain of MSL10 is not required for its**
395 **phosphorylation-dependent induction of cell death.** The region of homology
396 between the bacterial channel MscS and MSL10 is relatively small and comprises the
397 most C-terminal TM helix of each protein and subsequent 100 amino acids (Figure 2). In
398 MscS, these sequences form the channel pore and the upper vestibule of the
399 cytoplasmic domain. The corresponding portion of MSL10 is therefore likely to be
400 essential for its function as a MS channel. To test this, we expressed in Xenopus
401 oocytes a version of MSL10 that included the N-terminal cytoplasmic domain and the
402 first four TM helices (MSL10$_{1-316}$, Figure 5A) fused to YFP. MSL10$_{1-316}$-YFP was
403 expressed well and localized to the plasma membrane, but no mechanically activated
404 channel activity was detected (17 patches pulled from 6 oocytes), even at membrane
405 tensions that were close to lytic (Figure 5B). To determine if the MscS homology domain
406 of MSL10 was required to induce cell death, we transiently overexpressed MSL10$^{7A}{}_{1-316}$,
407 and MSL10$^{7D}{}_{1-316}$ fused to GFP in tobacco leaves. Truncation of MSL10 at amino acid
408 316 did not appreciably alter its expression level or its localization (Figure 5C).
409 Furthermore, as shown in Figure 5D, transient overexpression of MSL10$^{7A}{}_{1-316}$-GFP
410 (group c) caused even more cell death than the full-length channel MSL10^{7A}-GFP
411 (group a), while the cell death observed in leaf cells overexpressing MSL10$^{7D}{}_{1-316}$-GFP
412 was statistically indistinguishable from that induced by expression of full-length
413 MSL10^{7D}-GFP or *p19* alone (group b). We conclude that the ability of MSL10 to promote
414 cell death in a phosphorylation state-specific manner is genetically and physically
415 separable from its MscS homology domain and from its activity as a mechanosensitive
416 ion channel, a conclusion that is further supported below.

417

418 **The cytoplasmic N-terminal domain of MSL10 is sufficient to induce cell**
419 **death in tobacco.** To further delineate the portion of MSL10 responsible for the
420 production of phosphorylation-dependent cell death, we performed an analysis similar to
421 that shown in Figure 5, but with only the soluble N-terminal domain of MSL10 (aa 1-164,
422 Figure 6A) fused to GFP ($MSL10_{1-164}$-GFP). As expected, transient overexpression of
423 the full-length channel $MSL10^{7A}$-GFP caused a large percentage (approximately 50%)
424 of the cells to die (group a, Figure 6C), while expression of full-length $MSL10^{7D}$-GFP
425 produced the same amount of cell death as *p19* alone (group b). To our surprise,
426 $MSL10_{1-164}$-GFP was capable of inducing cell death to the same degree as the full-
427 length $MSL10^{7A}$-GFP protein (group a, Figure 6C). Furthermore, all three variants tested
428 ($MSL10_{1-164}$,-GFP, $MSL10^{7A}{}_{1-164}$-GFP, and $MSL10^{7D}{}_{1-164}$-GFP) caused the same level of
429 cell death (group a, Figure 6C). Thus, the soluble N-terminal domain of MSL10 is
430 capable of inducing cell death to the same degree as the full-length protein when
431 overexpressed in plant cells, but is no longer governed by phosphorylation state. All
432 three variants of the soluble N-terminal domain localized to the cytoplasm and nucleus
433 (the latter indicated by 4',6-diamidino-2-phenylindole (DAPI) signal (Figure 6B, bottom
434 row)). Full-length MSL10-GFP variants localized to the cell periphery as previously
435 observed (Figure 6B, top row). These data show that the N-terminal domain of MSL10
436 has cell death-promoting activity that does not require the pore-forming portion of the
437 channel or even tethering to the plasma membrane. Furthermore, physical separation
438 from the rest of the channel relieved the dependence of this activity on
439 dephosphorylation. The *in silico* simulations of protein folding presented in
440 Supplemental Figure 6 online are consistent with these conclusions, as they show the
441 cytoplasmic N-terminal domain forming a stable structure, and no gross structural
442 rearrangements associated with different phosphorylation states.

443

444 **DISCUSSION**

445 While little is known about members of the MscS family in multicellular eukaryotes, we
446 have previously speculated that the diversity of domains and topological complexity
447 present in the family may allow for unique functions and regulatory mechanisms to

448 evolve, each attuned to the needs of the organism in question. Further, we have
449 suggested that such unique functions might not be restricted to the release of osmolytes
450 (Haswell et al., 2011; Wilson et al., 2013). The data presented here provide support for
451 these ideas, employing as a test case the MscS-Like MS channel MSL10 from
452 *Arabidopsis thaliana*. We show that MSL10 is capable of acting as both a MS ion
453 channel and as a promoter of ROS accumulation and cell death. We further show that
454 the latter activity can be attributed to the soluble N-terminal domain of MSL10, and that
455 it is negatively regulated by phosphorylation of several serine and threonine residues.
456 These results pose a new set of questions; below we discuss some of these questions
457 and describe a working model that explains our observations and provides a platform
458 from which to begin future investigations.
459
460 **MSL10 as a sensor of membrane tension with multiple outputs.** In the work
461 presented here, we show that a cell-death-associated function of MSL10 is tied to a
462 plant-specific region of the protein and is regulated by phosphorylation. As the cell
463 death-inducing activity of MSL10 remained intact even after the removal of its
464 mechanosensitive capabilities, MSL10 can be considered to have at least two
465 genetically separable outputs—ion flux and triggering cell death. However, it is
466 reasonable to suppose that there is a functional link between the two. Our working
467 model for MSL10 function is presented in Figure 7. Like *E. coli* MscS, MSL10 is capable
468 of releasing osmolytes immediately in response to membrane tension. However, unlike
469 MscS, MSL10 is also capable of inducing cell death, and we hypothesize that this
470 activity is also normally activated in response to membrane tension. These two
471 responses could provide both a short- and a more long-term response to membrane
472 deformation. In a multicellular eukaryote like Arabidopsis, the subset of cells most
473 affected by mechanical stress might be sacrificed for the greater good of the entire
474 organism, as in the initiation of localized programmed cell death during the
475 hypersensitive response to pathogenic invasion (Coll et al., 2011; Senthil-Kumar and
476 Mysore, 2013). This idea is supported by the observation that, while hypoosmotic shock
477 causes cell death in bacteria due to lysis (Levina et al., 1999), eukaryotic cells respond
478 to hypoosmotic shock by undergoing a regulated process of cell death (Okada et al.,

479 2001; Nakayama et al., 2012). Figure 7 illustrates a model wherein the structural
480 rearrangements associated with increased membrane tension lead to both opening of
481 the channel pore (and thereby to ion flux across the membrane) and to exposure of the
482 N-terminal domain to a phosphatase (and thereby to its cell death promoting activity).
483 However, our data do not rule out the possibility that the ion channel activity of MSL10
484 is indirectly involved in the dephosphorylation of the soluble N-terminal domain. Below
485 we propose and discuss a few questions we aim to address in future work.
486
487 **How does dephosphorylation of the MSL10 N-terminal domain trigger cell death?**
488 Though it is not clear under what circumstances MSL10 is dephosphorylated *in vivo*, our
489 data provide some clues as to the potential mechanisms involved. Inhibition of MSL10's
490 cell death-promoting activity by phosphorylation was relieved when the soluble N-
491 terminal domain was expressed alone (compare Figures 5 and 6). Perhaps
492 dephosphorylation of the MSL10 N-terminal domain activates its cell death promoting
493 activity by favoring a structural rearrangement or the removal of a phospho-binding
494 protein (Oecking and Jaspert, 2009; Bozoky et al., 2013; Yamada et al., 2013).
495 According to this explanation, the active conformation would be favored when the
496 soluble N-terminal domain is expressed in the absence of the rest of MSL10.
497 Alternatively, dephosphorylation of the MSL10 N-terminal domain might lead to its
498 cleavage from the rest of the protein, as recently shown for the ER membrane-bound
499 EIN2 in response to ethylene (Ju et al., 2012). The cleaved protein would then be free
500 to activate cell death pathways in the cytoplasm or the nucleus. This would be mimicked
501 by expressing the soluble N-terminal domain on its own, consistent with the results
502 shown in Figure 6. As attractive as this explanation is, we have been unable to obtain
503 direct evidence for it. The lower molecular weight bands seen in MSL10-GFP
504 immunoblots (Figure 1E and 3C) were neither consistently observed nor associated with
505 phosphorylation state. As cleavage could take place anywhere in the soluble N-terminal
506 domain, and could be very inefficient, it remains possible that the cleaved version
507 cannot be distinguished from the wild type or even detected by immunoblot. We
508 attempted to identify cleavage products using a version of MSL10 that was tagged with
509 YFP at the N-terminus, but found that it was not properly expressed or trafficked in our

510 transient expression system (Supplemental Figure 7 online). Thus, MSL10-specific
511 antibodies must be developed in order to more rigorously test the cleavage model.
512
513 **What form(s) of cell death are induced by the MSL10 N-terminal domain?**
514 Plant cells can initiate the process of cell death in response to developmental signals,
515 abiotic stress, and pathogenic invasion. Plant cell death can take several forms, in some
516 cases resembling processes that have been identified in mammalian cells such as
517 apoptosis, autophagy, necrosis, and/or senescence (van Doorn and Woltering, 2005;
518 Reape and McCabe, 2008; Coll et al., 2011). The specific pathway activated in
519 Arabidopsis or tobacco cells overexpressing MSL10 variants is unclear and might
520 involve one or several of the following cell death mechanisms: activation of nuclear
521 endonucleases, activation of caspase-like or metacaspase proteases, loss of
522 mitochondrial integrity, or targeting of proteins or organelles to the autophagosome
523 (Lam et al., 2001; Coll et al., 2011; Liu and Bassham, 2012). It is notable that ROS
524 production and/or PCD have been documented in response to mechanical stimuli during
525 lateral root emergence (Mergemann and Sauter, 2000; Steffens et al., 2012), osmotic
526 shock response (Okada et al., 2001; Nakayama et al., 2012), immunity (Dodds and
527 Rathjen, 2010; Coll et al., 2011; Xin and He, 2013) and abiotic stress (Gill and Tuteja,
528 2010; Choi et al., 2013), suggesting that ROS-associated programmed cell death is a
529 common response to mechanical stress. While we cannot completely exclude the
530 possibility that the observed phenotypes do not reflect the normal function of MSL10,
531 we can conclude that they are unlikely to be simply the result of ER stress-induced cell
532 death (Tabas and Ron, 2011), as $MSL10^{D}$-GFP accumulated to the same or higher
533 levels as MSL10-GFP, showed similar subcellular localization, but did not appreciably
534 alter cell viability, plant growth or health.
535
536 In conclusion, we have shown that the cytoplasmic N-terminal domain of MSL10 is
537 capable of inducing cell death, that this activity is regulated by phosphorylation, and that
538 MSL10 has therefore two separable functions—one as an ion channel and one as an
539 inducer of cell death. These data provide support for our previous speculations that
540 MSL10 is more than a simple osmotic safety valve. Future studies will help us better

541 understand the diversity of ways in which MS channels have been employed as sensors
542 of membrane tension in plant and bacterial systems.
543
544 **METHODS**
545 ***Plant materials and growth conditions.*** Arabidopsis plants were grown on soil
546 at 21°C under a 24-hour light regime (approximately 150 µmol m−2 s−1). Cell size of
547 adaxial epidermal pavement cells from the fourth youngest leaf of 3-week-old plants
548 was assessed using ImageJ (http://imagej.nih.gov). For each background n > 100 cells
549 from 5 individual plants were counted, two leaves per plant. Transient overexpression of
550 *MSL10-GFP* variants in tobacco was performed as described (Waadt and Kudla, 2008).
551 For subcellular localization, organelle-specific (PM and ER) markers fused to the
552 fluorophore mCherry (Nelson et al., 2007) were co-infiltrated with MSL10-GFP and
553 visualized by CLSM 3 days post-infiltration. Tobacco tissue was subjected to
554 plasmolysis for 5 min in 1 M NaCl to induce Hechtian strands.
555 ***Cloning and transgenic lines.*** All plasmid constructs were made with Gateway
556 technology (Life Technologies). The MSL10 cDNA was cloned previously into
557 pENTR/D-TOPO (Haswell et al., 2008). This clone was used as a template for making
558 all MSL10 variants by the introduction of point mutations via site-directed mutagenesis
559 as described (Jensen and Haswell, 2012). These pENTR constructs were then used in
560 recombination reactions with pK7FWG2, (Karimi et al., 2002) to create C-terminal GFP-
561 fusion overexpression constructs (*P35S:MSL10-GFP*). The same constructs were used
562 to make stably transformed *Arabidopsis thaliana* lines and for transient expression in
563 *Nicotiana benthamiana*. For the generation of homozygous transgenic lines, Col-0
564 plants were transformed with by Agrobacterium-mediated transformation and T1 lines
565 were selected on agar-solidified MS medium (2 g/L Murashige and Skoog salts
566 (Caisson Labs)), pH 5.7 and 0.8% agar (Caisson Labs)) supplemented with kanamycin
567 (50 µg/ml). For testing the MSL10 variants in Xenopus oocytes, the gateway cassette-
568 containing region from pEarleyGate101 (Earley et al., 2006), which includes a C-
569 terminal YFP fusion, was amplified from the plasmid using the primers 5'–
570 TCTAGACATTTGGAGAGGACACG–3' and 5'-GATATCATTAAAGCAGGACTCTAGG-
571 3' and introduced into the expression vector pOO2 (Maksaev and Haswell, 2011)

572 between the XbaI and EcoRV sites. The same pENTR constructs containing MSL10
573 variants were used in recombination experiments with the YFP-containing pOO2 vector.
574 ***RT-PCR.*** Whole rosette tissue from three-week-old Arabidopsis was frozen in
575 liquid nitrogen. RNA isolation was performed using Trizol reagent as directed by the
576 manufacturer and 200 ng RNA was used for subsequent cDNA synthesis with oligo dT
577 primers and RT-PCR analysis. The oligos used to assess transcriptional activation for
578 each gene are listed in Supplemental Table 2 online. PCR products were separated on
579 a 2% agarose gel and imaged with ethidium bromide.
580 ***Yeast two-hybrid.*** Protein-protein interactions were assessed using the mating-
581 based split ubiquitin yeast two-hybrid system as described (Obrdlik et al., 2004). This
582 system was made available through the Arabidopsis Biological Resource Center and
583 the procedure was performed essentially as described in the manual provided with the
584 system. Briefly, *MSL10* cDNA, either with or without the phospho-point mutations
585 described above, was cloned by homologous recombination into either the THY.AP4
586 strain, carrying the plasmid *pMetYCgate*, or the THY.AP5 strain, carrying the plasmid
587 *pNXgate33-3HA*. The plasmid-containing cells were then mated and diploids were
588 selected on the appropriate dropout media. Interaction was determined by growth after
589 3 days on minimal media supplemented with 400 μM methionine to decrease
590 background growth.
591 ***Cell death, tissue staining, and microscopy.*** Confocal laser scanning
592 microscopy (CLSM) was performed using a Fluoview FV-1000 (Olympus), and images
593 were captured with FVIO-ASW software (Olympus). Dual staining with fluorescein
594 diacetate (FDA) and propidium iodide (PI) was used to quantify cell death (Chaves et
595 al., 2002) in *Nicotiana benthamiana* leaf cells transiently expressing MSL10 variants.
596 FDA is a fluorescent indicator of cell viability, as living cells process FDA to produce a
597 fluorescent compound within the cytoplasm (signal excited at 488 nm and emissions
598 collected with a 505 to 525 band-pass filter). PI preferentially penetrates cells with
599 damaged cell membranes, marking the nucleus and other intracellular compartments in
600 dead cells only (signal excited at 543 nm and emissions collected with a 560 to 660 nm
601 band-pass filter). Before each experiment, MSL10-GFP variant expression throughout
602 the leaf was verified by confocal imaging 5 days post-infiltration. Then, leaf samples

603 were immersed in staining solution (500 µg/ml FDA (5 mg/ml stock dissolved in
604 acetone) and 1.25 µg/ml PI (2.5 mg/ml stock dissolved in water)) for 20 minutes before
605 rinsing with water and imaging of the abaxial epidermis. Images of randomized samples
606 were collected and cell death quantified. Pavement cells were classified as "alive"
607 unless they fulfilled one or more of the following criteria: 1) the presence of PI-staining
608 in the nucleus; 2) other PI-staining particles or compartments in the cell center or 3) the
609 disappearance of a clear vacuole, accompanied by spreading of cytoplasmic GFP/FDA
610 signal. Images illustrating each of these are shown in Supplemental Figure 4. n > 120
611 cells were counted from each construct from two to three separate infiltration
612 experiments, each consisting of 3 infiltrated leaves. Statistical differences were
613 analyzed by one-way ANOVA and Tukey's test, and groups that did not differ
614 significantly were noted ($p < 0.05$). For DAPI staining, 4',6-diamidino-2-phenylindole (5
615 ug/mL) was dissolved in water with 0.1% Silwet to aid in the penetration of the stain,
616 and leaf samples were floated in the solution for 20 min before imaging. DAPI was
617 excited with a 405 nm laser and emission was collected using a 430 to 470 nm band-
618 pass filters. For subcellular-localization experiments, mCherry was excited with a 543
619 nm laser and emission was collected using a 560 to 660 nm band-pass filters. Staining
620 with 3,3'-Diaminobenzidine (DAB) for H_2O_2 production was performed on leaf 4 or 5
621 from 2-week-old plants as described (Mahalingam et al., 2006). Trypan blue staining for
622 lesion formation was performed on leaf number 12-14 on 3-week-old plants as
623 described (Vogel and Somerville, 2000).

624 ***Oocyte preparation.*** Oocytes from *Xenopus laevis* (Dumont stage V or VI)
625 females were isolated as previously described (Yang and Sachs, 1990; Stühmer and
626 Parekh, 1995) and incubated in ND96 buffer (96 mM NaCl, 2 mM KCl, 1.8 mM $CaCl_2$, 1
627 mM $MgCl_2$, 5 mM Hepes, pH 7.4) with 50 mg/l gentamicin at 18°C overnight. The day
628 after isolation, cells were injected with 50 nl of 1 µg/µl cRNA and were patched 7-14
629 days after injection. Prior to patching, vitelline membranes were removed from the
630 oocytes with a pair of dull forceps.

631 ***Electrophysiology.*** De-vitellinized oocytes were patched in symmetric modified
632 ND96 buffer (96 mM NaCl, 2 mM KCl, 1.8 mM $CaCl_2$, 10 mM $MgCl_2$, 5 mM Hepes, pH
633 7.4) using pipette bubble number 4.5-5 in the inside-out (excised) patch configuration.

634 Pressure ramps were generated by a High Speed Pressure System (HSPS-1, ALA
635 Sciences). The micromanipulator system Scientifica PatchStar 700 was used for
636 membrane patching (Scientifica, UK). Data were acquired at 20 kHz, filtered at 5 kHz
637 and digitized with the Axopatch 200B patch-clamp amplifier and the Digidata 1440A
638 digitizer (Molecular Devices) and further analyzed with the pClamp10 software suite
639 (Molecular Devices). Pipettes were fabricated of Kimax 51 patch glass (Kimble
640 Products) using a Sutter P-97 puller (Sutter Instruments). Measurements were made on
641 at least 3 oocytes for the wild-type protein and each mutant selected from at least 2
642 different batches of cells. Recordings were made at -30 to -40mV membrane potentials
643 and -40 to -200 mmHg transmembrane pressures, while mechanosensitive activity
644 typically began to appear at -60 to -70 mm Hg pressure.
645 ***Immunoblot analysis.*** Total plant protein ground in 2X sample buffer was used
646 for western analysis. The proteins were denatured for 5 min at 97°C, separated by SDS-
647 PAGE (100V for 2.5 hours), and transferred to PVDF membrane. After overnight
648 blocking in TBST (10 mM Tris-Cl, 150 mM NaCl, 0.05% (v/v) Tween20, pH 7.5) with 5%
649 (wt/v) non-fat milk powder, the membrane was incubated for 1 hour with primary anti-
650 GFP antibody (Clontech) at room temperature. Then the membrane was treated with
651 anti-mouse secondary antibodies for 1 hour at room temperature. Detection was
652 performed using Thermo Scientific Femto detection kit (Thermo Scientific) and BioMax
653 XAR film (Kodak). Blots were subsequently stripped and re-probed as above with anti-α-
654 tubulin antibody (Sigma) to assess loading.
655
656 **ACKNOWLEDGEMENTS**
657 This work was supported by National Science Foundation MCB1253103, National
658 Institutes of Health GM084211 and NASA NNX13AM55G (to E.S.H.), and the Howard
659 Hughes Medical Institute for a Summer Undergraduate Research Fellowship to S.K..
660 We acknowledge the Arabidopsis Biological Resource Center for making available the
661 split-ubiquitin yeast two-hybrid system and are grateful to the Washington University
662 greenhouse staff for their assistance.
663
664 **AUTHOR CONTRIBUTIONS**

665 Kira M. Veley – writing the manuscript, performed and designed experiments, data
666 analysis
667 Grigory Maksaev – writing the manuscript, performed and designed experiments, data
668 analysis
669 Elizabeth M. Frick – performed and designed experiments, data analysis
670 Emma January – performed experiments, data analysis
671 Sarah C. Kloepper – performed experiments, data analysis
672 Elizabeth S. Haswell – writing the manuscript, experimental design, data analysis
673
674 **FIGURE LEGENDS**
675 **Figure 1.** Phenotypes associated with the overexpression of *MSL10-GFP* in
676 Arabidopsis.
677 **(A)** Wild-type (WT, Col-0) plants, three independent homozygous transgenic T_2 lines
678 (also in the Col-0 background) expressing *MSL10-GFP* and two independent
679 homozygous T_2 lines expressing *MSL10^{4D}-GFP* from the Cauliflower Mosaic
680 Virus 35S promoter (*P35S*) are compared. Top row: images of 3-week-old plants
681 grown at 21°C under a 24 hour light regime. Bar = 0.5 cm. Middle row: Bright-
682 field images of leaf 4 or 5 from 2-week-old plants from the indicated lines stained
683 with 3,3'-Diaminobenzidine (DAB) for the presence of hydrogen peroxide. Bar =
684 0.1 cm. Bottom row: Bright-field images of leaf 4 or 5 from 2-week-old plants from
685 each line stained with trypan blue to assess lesion formation. Bar = 200 µm.
686 **(B)** RT-PCR analysis of selected genes in WT and *MSL10-GFP* overexpression
687 lines. cDNA was synthesized from RNA extracted from rosette tissue from 21-
688 day-old plants. *ACTIN* expression was used as a control.
689 **(C)** Average fresh weight (mg) of rosettes from ten 17-day-old soil-grown plants.
690 Error bars = standard deviation. * p value < 0.01 relative to Col (Student's *t*-test).
691 **(D)** Top: Representative confocal laser scanning microscopy (CLSM) images of cell
692 outlines analyzed by ImageJ. Samples were taken from the distal quadrant of the
693 4th newest leaf from three-week-old plants, and cells from the adaxial surface
694 were imaged. Bar = 50 µm. Bottom: Average area of n > 100 cells per

695 background. Error bars = standard deviation. * *p* value < 0.01 relative to WT
696 (Student's *t*-test).
697 **(E)** Immunoblot of extracts from the stably transformed Arabidopsis lines shown in
698 (A). Blot was detected with an anti-GFP primary antibody (top), then stripped and
699 re-probed with anti-α-tubulin primary antibody (bottom). Protein sizes are
700 indicated at the right according to a commercially available standard.
701
702 **Figure 2.** Predicted topology of a MSL10 monomer.
703 Cartoon of the predicted topology of MSL10 as predicted by ARAMEMNON
704 (http://aramemnon. botanik.uni-koeln.de). Each circle represents an individual amino
705 acid. The lipid bilayer is indicated by a grey bar, with the cytoplasmic domains of the
706 protein underneath. The MscS homology domain is indicated in dark blue. The
707 cytoplasmic N-terminal domain is dark red and the phosphorylated residues within it
708 are black and the residue numbers indicated. The conditions under which each
709 residue has been found to be phosphorylated, the phosphopeptide context for each
710 and associated references can be found in Supplemental Table 1 online.
711
712 **Figure 3.** Quantification of cell death in tobacco cells transiently expressing MSL10-
713 GFP variants.
714 **(A)** Images of the abaxial surface of tobacco leaves after infiltration with
715 Agrobacterium harboring the indicated MSL10-GFP variant and the
716 expression enhancer *p19*. Top row: CLSM image of GFP expression
717 (pseudocolored green) in epidermal cells 3 days post-infiltration. Bar = 50 µm.
718 Second row: GFP expression 5 days post-infiltration. Bar = 50 µm. Third row:
719 Bright-field images of tobacco leaf samples 5 days post-infiltration stained
720 with trypan blue to assess lesion formation. Bar = 500 µm. Bottom row:
721 Representative images of live and dead pavement cells in tobacco leaves 5
722 days after infiltration. Leaves were stained with fluorescein diacetate (FDA,
723 pseudocolored yellow) and propidium iodide (PI, pseudocolored red). The left
724 panel is a representative example of an image showing cells scored as

725 “dead”, due to PI staining in the nucleus and lack of FDA or GFP signal, while
726 all cells shown in the right panel were scored as “live”. Bar = 10 μm.
727 **(B)** Percentage of dead cells in tissue expressing MSL10-GFP variants co-
728 infiltrated with *p19*. At least 120 cells were counted from each construct from
729 two separate infiltration experiments, each consisting of three infiltrated
730 leaves. Statistical differences were analyzed by one-way ANOVA and Tukey’s
731 test, and groups that did not differ significantly are indicated by the same
732 letter (a and b, $p < 0.05$). *p19* alone was used as a background control.
733 **(C)** Immunoblot analysis of MSL10-GFP from samples used in one of the tobacco
734 expression experiments in (B). Protein extracts from leaves infiltrated with
735 *p19* alone were used as a negative control. Top: Anti-GFP antibody. Bottom:
736 Anti-α-tubulin loading control. The migration of bands from a commercially
737 available protein size standard is indicated at the right.
738
739 **Figure 4.** Effect of phosphomimetic and alanine substitution mutations on MSL10
740 behavior.
741 **(A)** Subcellular localization in epidermal cells from tobacco transiently expressing
742 the same GFP constructs stably transformed into Arabidopsis. CLSM images
743 were taken 3 days post-infiltration, before high levels of cell death were seen.
744 To assess subcellular localization, MSL10 variants were co-infiltrated with
745 either an ER (ER-mCherry) or a plasma membrane (PM-mCherry) marker
746 (Nelson et al., 2007). MSL10-GFP was pseudocolored green and the ER
747 marker (top row) or the PM marker (middle row) were pseudocolored
748 magenta; co-localization appears white. Bottom row: MSL10-GFP-expressing
749 cells were plasmolyzed for 5 min in 5 M NaCl. Arrowheads indicate GFP
750 signal in Hechtian strands. Bars = 10 μm.
751 **(B)** Split-ubiquitin yeast two-hybrid analysis of protein-protein interactions among
752 WT and mutant forms of MSL10. Each variant of MSL10 was fused to either
753 Cub (rows) or Nub (columns), and haploid yeast containing a single construct
754 were mated. Growth of diploid cells after 5 days on minimal media indicated
755 an interaction. The N-terminal half of ubiquitin alone (NubG) was used as a

756 negative control. The “G” in NubG indicates a mutation within Nub that
757 decreases the incidence of false positive interactions. WT Nub, which
758 contains no such mutation and is thus more promiscuous when used as a
759 binding partner, was used as a positive control.

760 **(C)** Top: CLSM images of the edge of Xenopus oocytes expressing MSL10-GFP
761 (pseudocolored green) 7-days after injection with cRNA. Mock injections with
762 water were used as a control. Bars = 100 μm. Bottom: Representative traces
763 of tension-induced currents in inside-out excised patches from Xenopus
764 oocytes expressing MSL10 variants. Records were made from the patches in
765 pipettes with BN ~ 5 in symmetric ND96 buffer. Membrane potentials were
766 clamped at -40 (WT) or -30 mV ($MSL10^{7A}$, $MSL10^{7D}$) during the application of
767 a symmetric triangular 5 sec pressure ramp to -70 (WT, $MSL10^{7A}$) or -60 mm
768 Hg ($MSL10^{7D}$). Note that hysteresis (wherein the last channel closes at lower
769 tensions than the first channel opens) was observed in all traces. A
770 quantification of opening threshold tension and open/close threshold tension
771 ratios is shown in Supplemental Figure 5 online.

772 **(D)** Current/voltage curves of MSL10-GFP (open circles), $MSL10^{7A}$-YFP
773 (diamonds), and $MSL10^{7D}$-YFP (closed circles) under membrane tension (n =
774 3 oocytes for each protein). The GFP tag does not alter MSL10 conductance
775 (Maksaev and Haswell, 2012).

776

777 **Figure 5.** Mechanosensitive ion channel activity of $MSL10_{1\text{-}316}$-GFP and its effects on
778 cell death and subcellular localization.

779 **(A)** Cartoon of the $MSL10_{1\text{-}316}$ monomer. Most of the cytoplasmic loop, the 5th and
780 the 6th TM helices, and the cytoplasmic C-terminus are deleted. These
781 deleted portions include the MscS homology domain, which forms the
782 channel pore in *E. coli* MscS.

783 **(B)** Top: Confocal scan of the periphery of the oocyte expressing $MSL10_{1\text{-}316}$-
784 GFP showing strong fluorescent signal. Image was taken 7 days after
785 injection of RNA. Bar = 100 μm. Bottom: A representative trace showing an

786 absence of mechanosensitive activity even at high transmembrane pressures.
787 The membrane potential was clamped at -50 mV.
788 **(C)** CLSM images of abaxial tobacco leaf epidermis from plants transiently
789 expressing variants of full length MSL10-GFP (top row) or $MSL10_{1-316}$-GFP
790 (bottom row). All seven phosphorylated residues were mutated as indicated
791 above each image. GFP signal is pseudocolored green. Images were taken 3
792 days post-infiltration. Bar = 50 μm.
793 **(D)** Percentage of dead cells in tissue expressing the same constructs as in (C) 5
794 days post-infiltration. The number and type of mutated residues is indicated
795 below each bar, and the *p19* plasmid alone was used as a negative control.
796 Cells were counted over two independent infiltration experiments, each
797 consisting of 3 infiltrated leaves per construct, n > 100. Statistical differences
798 were analyzed by one-way ANOVA and Tukey's test, and groups that differed
799 significantly are indicated by different letters (a, b, and c, *p* value < 0.05).
800
801 **Figure 6.** Effects of expressing the soluble N-terminal domain of MSL10 ($MSL10_{1-164}$-
802 GFP) on cell death and subcellular localization.
803 **(A)** Cartoon of $MSL10_{1-164}$. All six TM helices, the cytoplasmic loop between TM4
804 and TM5 and the C-terminal domain are deleted.
805 **(B)** CLSM images of the abaxial tobacco leaf epidermis from plants transiently
806 expressing either full length MSL10-GFP (top) or $MSL10_{1-164}$-GFP, (bottom), 3
807 days post-infiltration. The phosphovariant of MSL10 used in the infiltration is
808 indicated above each image. GFP signal is pseudocolored green and the
809 DNA marker DAPI pseudocolored blue. Co-localization of GFP and DAPI
810 signals appears aqua. Bar = 10 μm.
811 **(C)** Percentage of dead cells in tissue expressing the same constructs as in (B) 5
812 days post-infiltration. The number and type of mutated residues is indicated
813 below each bar, and the *p19* plasmid alone was used as a negative control.
814 Cells were counted over two separate infiltration experiments, each consisting
815 of 3 infiltrated leaves per construct. n > 100. Statistical differences were
816 analyzed by one-way ANOVA and Tukey's test, and groups that do not differ

817 significantly are indicated by the same letter (a, b, and c, *p* value < 0.05). *p19*
818 alone was used as a negative control.
819
820 **Figure 7.** Working model for MSL10 function and regulation.
821 Depicted are topological diagrams of *E. coli* MscS (left) and its *A. thaliana*
822 homolog MSL10 (right), both embedded in the plasma membrane. MscS is
823 known to function as an osmotic safety valve, releasing osmolytes in response to
824 increased membrane tension and preventing cells from lysing under hypoosmotic
825 shock (function 1). MSL10 also forms a channel that opens and releases ions in
826 response to increased membrane tension, in a manner that requires the MscS
827 homology domain (dark blue). The soluble N-terminal domain of MSL10 (brick
828 red), which is specific to MSL10 and its orthologs in plants, serves a second,
829 plant-specific function in the promotion of ROS production and cell death
830 (function 2). Only the second function is regulated by phosphorylation of seven
831 Ser and Thr residues located in the N-terminal domain.
832
833 **ACCESSION NUMBERS**
834 At5G12080, AT5G12080, AT5G45890, AT4G11650, AT3G01420, AT3G49120,
835 AT1G73260
836
837 **SUPPLEMENTAL DATA**
838 **Supplemental Figure 1.** Additional phenotypes associated with MSL10-GFP
839 overexpression.
840
841 **Supplemental Figure 2.** Multiple sequence alignment of the N-termini of MSL10
842 orthologs in land plants.
843
844 **Supplemental Figure 3.** Multiple sequence alignment of Class II MSL proteins from
845 *Arabidopsis thaliana* and MscS from *Escherichia coli*.
846

847 **Supplemental Figure 4.** Documentation of the cell death assay used in Figures 3, 5,
848 and 6.
849
850 **Supplemental Figure 5.** Electrophysiological analysis of MSL10 variants in Xenopus
851 ooctyes.
852
853 **Supplemental Figure 6.** Molecular dynamics simulations of the soluble N-terminal
854 domain of MSL10**.**
855
856 **Supplemental Figure 7.** Subcellular localization of N-terminally tagged full-length YFP-
857 MSL10 variants.
858
859 **Supplemental Table 1.** Experimentally determined *in vivo* phosphorylated peptides
860 attributed to the MSL10 N-terminus.
861
862 **Supplemental Table 2.** Primers used for RT-PCR.
863
864 **Supplemental Methods**
865
866 **Supplemental References**
867
868 **REFERENCES**
869 **Abdin, M.Z., Kiran, U., and Alam, A.** (2011). Analysis of osmotin, a PR protein as
870 metabolic modulator in plants. Bioinformation **5,** 336-340.
871 **Arnadottir, J., and Chalfie, M.** (2010). Eukaryotic mechanosensitive channels. Annu
872 Rev Biophys **39,** 111-137.
873 **Balleza, D., and Gomez-Lagunas, F.** (2009). Conserved motifs in mechanosensitive
874 channels MscL and MscS. Eur Biophys J **38,** 1013-1027.

875 **Bass, R.B., Strop, P., Barclay, M., and Rees, D.C.** (2002). Crystal structure of
876 Escherichia coli MscS, a voltage-modulated and mechanosensitive channel.
877 Science **298,** 1582-1587.
878 **Bayle, V., Arrighi, J.F., Creff, A., Nespoulous, C., Vialaret, J., Rossignol, M.,**
879 **Gonzalez, E., Paz-Ares, J., and Nussaume, L.** (2011). Arabidopsis thaliana
880 high-affinity phosphate transporters exhibit multiple levels of posttranslational
881 regulation. Plant Cell **23,** 1523-1535.
882 **Belyy, V., Anishkin, A., Kamaraju, K., Liu, N., and Sukharev, S.** (2010). The tension-
883 transmitting 'clutch' in the mechanosensitive channel MscS. Nat Struct Mol Biol
884 **17,** 451-458.
885 **Benschop, J.J., Mohammed, S., O'Flaherty, M., Heck, A.J., Slijper, M., and Menke,**
886 **F.L.** (2007). Quantitative phosphoproteomics of early elicitor signaling in
887 Arabidopsis. Mol Cell Proteomics **6,** 1198-1214.
888 **Bindschedler, L.V., Dewdney, J., Blee, K.A., Stone, J.M., Asai, T., Plotnikov, J.,**
889 **Denoux, C., Hayes, T., Gerrish, C., Davies, D.R., Ausubel, F.M., and Bolwell,**
890 **G.P.** (2006). Peroxidase-dependent apoplastic oxidative burst in Arabidopsis
891 required for pathogen resistance. Plant J **47,** 851-863.
892 **Blanco, F., Garreton, V., Frey, N., Dominguez, C., Perez-Acle, T., Van der Straeten,**
893 **D., Jordana, X., and Holuigue, L.** (2005). Identification of NPR1-dependent and
894 independent genes early induced by salicylic acid treatment in Arabidopsis. Plant
895 Mol Biol **59,** 927-944.
896 **Blount, P., and Moe, P.C.** (1999). Bacterial mechanosensitive channels: integrating
897 physiology, structure and function. Trends Microbiol **7,** 420-424.

898 **Boer, M., Anishkin, A., and Sukharev, S.** (2011). Adaptive MscS gating in the osmotic
899 permeability response in E. coli: the question of time. Biochemistry **50,** 4087-
900 4096.
901 **Bozoky, Z., Krzeminski, M., Chong, P.A., and Forman-Kay, J.D.** (2013). Structural
902 changes of CFTR R region upon phosphorylation: a plastic platform for
903 intramolecular and intermolecular interactions. FEBS Journal**,** n/a-n/a.
904 **Brusslan, J.A., Rus Alvarez-Canterbury, A.M., Nair, N.U., Rice, J.C., Hitchler, M.J.,**
905 **and Pellegrini, M.** (2012). Genome-wide evaluation of histone methylation
906 changes associated with leaf senescence in Arabidopsis. PLoS One **7,** e33151.
907 **Capelli, N., Diogon, T., Greppin, H., and Simon, P.** (1997). Isolation and
908 characterization of a cDNA clone encoding an osmotin-like protein from
909 Arabidopsis thaliana. Gene **191,** 51-56.
910 **Chaves, I., Regalado, A.P., Chen, M., Ricardo, C.P., and Showalter, A.M.** (2002).
911 Programmed cell death induced by (β-d-galactosyl)3 Yariv reagent in Nicotiana
912 tabacum BY-2 suspension-cultured cells. Physiologia Plantarum **116,** 548-553.
913 **Choi, D.S., Hong, J.K., and Hwang, B.K.** (2013). Pepper osmotin-like protein 1
914 (CaOSM1) is an essential component for defense response, cell death, and
915 oxidative burst in plants. Planta.
916 **Claeys, H., Van Landeghem, S., Dubois, M., Maleux, K., and Inze, D.** (2014). What is
917 Stress? Dose-Response Effects in Commonly Used In Vitro Stress Assays. Plant
918 Physiol.
919 **Coll, N.S., Epple, P., and Dangl, J.L.** (2011). Programmed cell death in the plant
920 immune system. Cell Death Differ **18,** 1247-1256.

921 **Cox, C.D., Nakayama, Y., Nomura, T., and Martinac, B.** (2014). The evolutionary
922 'tinkering' of MscS-like channels: generation of structural and functional diversity.
923 Pflugers Arch.
924 **Cox, C.D., Nomura, T., Ziegler, C.S., Campbell, A.K., Wann, K.T., and Martinac, B.**
925 (2013). Selectivity mechanism of the mechanosensitive channel MscS revealed
926 by probing channel subconducting states. Nat Commun **4,** 2137.
927 **Cui, M.H., Ok, S.H., Yoo, K.S., Jung, K.W., Yoo, S.D., and Shin, J.S.** (2013). An
928 Arabidopsis cell growth defect factor-related protein, CRS, promotes plant
929 senescence by increasing the production of hydrogen peroxide. Plant Cell
930 Physiol **54,** 155-167.
931 **Cui, Y., Zhang, M., Pestell, R., Curran, E.M., Welshons, W.V., and Fuqua, S.A.**
932 (2004). Phosphorylation of estrogen receptor alpha blocks its acetylation and
933 regulates estrogen sensitivity. Cancer Res **64,** 9199-9208.
934 **Daudi, A., Cheng, Z., O'Brien, J.A., Mammarella, N., Khan, S., Ausubel, F.M., and**
935 **Bolwell, G.P.** (2012). The apoplastic oxidative burst peroxidase in Arabidopsis is
936 a major component of pattern-triggered immunity. Plant Cell **24,** 275-287.
937 **De Leon, I.P., Sanz, A., Hamberg, M., and Castresana, C.** (2002). Involvement of the
938 Arabidopsis alpha-DOX1 fatty acid dioxygenase in protection against oxidative
939 stress and cell death. Plant J **29,** 61-62.
940 **Desikan, R., Reynolds, A., Hancock, J.T., and Neill, S.J.** (1998). Harpin and
941 hydrogen peroxide both initiate programmed cell death but have differential
942 effects on defence gene expression in Arabidopsis suspension cultures. Biochem
943 J **330 (Pt 1),** 115-120.

944 **Diaz, C., Saliba-Colombani, V., Loudet, O., Belluomo, P., Moreau, L., Daniel-**
945 **Vedele, F., Morot-Gaudry, J.F., and Masclaux-Daubresse, C.** (2006). Leaf
946 yellowing and anthocyanin accumulation are two genetically independent
947 strategies in response to nitrogen limitation in Arabidopsis thaliana. Plant Cell
948 Physiol **47,** 74-83.
949 **Dodds, P.N., and Rathjen, J.P.** (2010). Plant immunity: towards an integrated view of
950 plant-pathogen interactions. Nat Rev Genet **11,** 539-548.
951 **Earley, K.W., Haag, J.R., Pontes, O., Opper, K., Juehne, T., Song, K., and Pikaard,**
952 **C.S.** (2006). Gateway-compatible vectors for plant functional genomics and
953 proteomics. Plant J **45,** 616-629.
954 **Ebert, D.H., Gabel, H.W., Robinson, N.D., Kastan, N.R., Hu, L.S., Cohen, S.,**
955 **Navarro, A.J., Lyst, M.J., Ekiert, R., Bird, A.P., and Greenberg, M.E.** (2013).
956 Activity-dependent phosphorylation of MECP2 threonine 308 regulates
957 interaction with NcoR. Nature.
958 **Engelsberger, W.R., and Schulze, W.X.** (2012). Nitrate and ammonium lead to distinct
959 global dynamic phosphorylation patterns when resupplied to nitrogen-starved
960 Arabidopsis seedlings. The Plant Journal **69,** 978-995.
961 **Fischer-Kilbienski, I., Miao, Y., Roitsch, T., Zschiesche, W., Humbeck, K., and**
962 **Krupinska, K.** (2010). Nuclear targeted AtS40 modulates senescence
963 associated gene expression in Arabidopsis thaliana during natural development
964 and in darkness. Plant Mol Biol **73,** 379-390.

965 **Gamini, R., Sotomayor, M., Chipot, C., and Schulten, K.** (2011). Cytoplasmic domain
966 filter function in the mechanosensitive channel of small conductance. Biophys J
967 **101,** 80-89.
968 **Gan, S., and Amasino, R.M.** (1997). Making Sense of Senescence (Molecular Genetic
969 Regulation and Manipulation of Leaf Senescence). Plant Physiol **113,** 313-319.
970 **Garabagi, F., Gilbert, E., Loos, A., McLean, M.D., and Hall, J.C.** (2012). Utility of the
971 P19 suppressor of gene-silencing protein for production of therapeutic antibodies
972 in Nicotiana expression hosts. Plant Biotechnol J **10,** 1118-1128.
973 **Gill, S.S., and Tuteja, N.** (2010). Reactive oxygen species and antioxidant machinery in
974 abiotic stress tolerance in crop plants. Plant Physiol Biochem **48,** 909-930.
975 **Haswell, E.S., and Meyerowitz, E.M.** (2006). MscS-like proteins control plastid size
976 and shape in Arabidopsis thaliana. Curr Biol **16,** 1-11.
977 **Haswell, E.S., Phillips, R., and Rees, D.C.** (2011). Mechanosensitive channels: what
978 can they do and how do they do it? Structure **19,** 1356-1369.
979 **Haswell, E.S., Peyronnet, R., Barbier-Brygoo, H., Meyerowitz, E.M., and Frachisse,**
980 **J.M.** (2008). Two MscS homologs provide mechanosensitive channel activities in
981 the Arabidopsis root. Curr Biol **18,** 730-734.
982 **Jefferson, R.A., Kavanagh, T.A., and Bevan, M.W.** (1987). GUS fusions: beta-
983 glucuronidase as a sensitive and versatile gene fusion marker in higher plants.
984 EMBO J **6,** 3901-3907.
985 **Jensen, G.S., and Haswell, E.S.** (2012). Functional analysis of conserved motifs in the
986 mechanosensitive channel homolog MscS-Like2 from Arabidopsis thaliana. PLoS
987 One **7,** e40336.

988 **Ju, C., Yoon, G.M., Shemansky, J.M., Lin, D.Y., Ying, Z.I., Chang, J., Garrett, W.M.,**
989 **Kessenbrock, M., Groth, G., Tucker, M.L., Cooper, B., Kieber, J.J., and**
990 **Chang, C.** (2012). CTR1 phosphorylates the central regulator EIN2 to control
991 ethylene hormone signaling from the ER membrane to the nucleus in
992 Arabidopsis. Proc Natl Acad Sci U S A **109,** 19486-19491.
993 **Karimi, M., Inze, D., and Depicker, A.** (2002). GATEWAY vectors for Agrobacterium-
994 mediated plant transformation. Trends Plant Sci **7,** 193-195.
995 **Kaufman, R.J., Davies, M.V., Pathak, V.K., and Hershey, J.W.** (1989). The
996 phosphorylation state of eucaryotic initiation factor 2 alters translational efficiency
997 of specific mRNAs. Mol Cell Biol **9,** 946-958.
998 **Kloda, A., and Martinac, B.** (2002). Common evolutionary origins of mechanosensitive
999 ion channels in Archaea, Bacteria and cell-walled Eukarya. Archaea **1,** 35-44.
1000 **Koprowski, P., Grajkowski, W., Isacoff, E.Y., and Kubalski, A.** (2011). Genetic
1001 screen for potassium leaky small mechanosensitive channels (MscS) in
1002 Escherichia coli: recognition of cytoplasmic beta domain as a new gating
1003 element. J Biol Chem **286,** 877-888.
1004 **Kotchoni, S.O., and Gachomo, E.W.** (2006). The reactive oxygen species network
1005 pathways:an essential prerequisite for perception of pathogen attack and the
1006 acquired disease resistance in plants. J Biosci **31,** 389-404.
1007 **Koyama, T., Nii, H., Mitsuda, N., Ohta, M., Kitajima, S., Ohme-Takagi, M., and Sato,**
1008 **F.** (2013). A regulatory cascade involving class II ETHYLENE RESPONSE
1009 FACTOR transcriptional repressors operates in the progression of leaf
1010 senescence. Plant Physiol **162,** 991-1005.

1011 **Kung, C., Martinac, B., and Sukharev, S.** (2010). Mechanosensitive channels in
1012 microbes. Annu Rev Microbiol **64,** 313-329.
1013 **Lai, J.Y., Poon, Y.S., Kaiser, J.T., and Rees, D.C.** (2013). Open and shut: crystal
1014 structures of the dodecylmaltoside solubilized mechanosensitive channel of small
1015 conductance from Escherichia coli and Helicobacter pylori at 4.4 A and 4.1 A
1016 resolutions. Protein Sci **22,** 502-509.
1017 **Lam, E., Kato, N., and Lawton, M.** (2001). Programmed cell death, mitochondria and
1018 the plant hypersensitive response. Nature **411,** 848-853.
1019 **Latz, A., Becker, D., Hekman, M., Muller, T., Beyhl, D., Marten, I., Eing, C., Fischer,**
1020 **A., Dunkel, M., Bertl, A., Rapp, U.R., and Hedrich, R.** (2007). TPK1, a Ca(2+)-
1021 regulated Arabidopsis vacuole two-pore K(+) channel is activated by 14-3-3
1022 proteins. Plant J **52,** 449-459.
1023 **Levina, N., Totemeyer, S., Stokes, N.R., Louis, P., Jones, M.A., and Booth, I.R.**
1024 (1999). Protection of Escherichia coli cells against extreme turgor by activation of
1025 MscS and MscL mechanosensitive channels: identification of genes required for
1026 MscS activity. EMBO J **18,** 1730-1737.
1027 **Li, C., Edwards, M.D., Jeong, H., Roth, J., and Booth, I.R.** (2007). Identification of
1028 mutations that alter the gating of the Escherichia coli mechanosensitive channel
1029 protein, MscK. Mol Microbiol **64,** 560-574.
1030 **Li, H., Wong, W.S., Zhu, L., Guo, H.W., Ecker, J., and Li, N.** (2009).
1031 Phosphoproteomic analysis of ethylene-regulated protein phosphorylation in
1032 etiolated seedlings of Arabidopsis mutant ein2 using two-dimensional

1033 separations coupled with a hybrid quadrupole time-of-flight mass spectrometer.
1034 Proteomics **9,** 1646-1661.
1035 **Li, J., Brader, G., and Palva, E.T.** (2008). Kunitz trypsin inhibitor: an antagonist of cell
1036 death triggered by phytopathogens and fumonisin b1 in Arabidopsis. Mol Plant **1,**
1037 482-495.
1038 **Li, Y., Moe, P.C., Chandrasekaran, S., Booth, I.R., and Blount, P.** (2002). Ionic
1039 regulation of MscK, a mechanosensitive channel from Escherichia coli. EMBO J
1040 **21,** 5323-5330.
1041 **Liu, Y., and Bassham, D.C.** (2012). Autophagy: pathways for self-eating in plant cells.
1042 Annu Rev Plant Biol **63,** 215-237.
1043 **Liu, Z., Walton, T.A., and Rees, D.C.** (2010). A reported archaeal mechanosensitive
1044 channel is a structural homolog of MarR-like transcriptional regulators. Protein
1045 Sci **19,** 808-814.
1046 **Ludewig, U., Wilken, S., Wu, B., Jost, W., Obrdlik, P., El Bakkoury, M., Marini, A.M.,**
1047 **Andre, B., Hamacher, T., Boles, E., von Wiren, N., and Frommer, W.B.**
1048 (2003). Homo- and hetero-oligomerization of ammonium transporter-1 NH4
1049 uniporters. J Biol Chem **278,** 45603-45610.
1050 **Mahalingam, R., Jambunathan, N., Gunjan, S.K., Faustin, E., Weng, H., and**
1051 **Ayoubi, P.** (2006). Analysis of oxidative signalling induced by ozone in
1052 Arabidopsis thaliana. Plant Cell Environ **29,** 1357-1371.
1053 **Maksaev, G., and Haswell, E.S.** (2011). Expression and characterization of the
1054 bacterial mechanosensitive channel MscS in Xenopus laevis oocytes. J Gen
1055 Physiol **138,** 641-649.

1056 **Maksaev, G., and Haswell, E.S.** (2012). MscS-Like10 is a stretch-activated ion channel
1057 from Arabidopsis thaliana with a preference for anions. Proc Natl Acad Sci U S A
1058 **109,** 19015-19020.
1059 **Malcolm, H.R., and Maurer, J.A.** (2012). The mechanosensitive channel of small
1060 conductance (MscS) superfamily: not just mechanosensitive channels anymore.
1061 Chembiochem **13,** 2037-2043.
1062 **Marin, M., Thallmair, V., and Ott, T.** (2012). The intrinsically disordered N-terminal
1063 region of AtREM1.3 remorin protein mediates protein-protein interactions. J Biol
1064 Chem **287,** 39982-39991.
1065 **Martinac, B.** (2011). Bacterial mechanosensitive channels as a paradigm for
1066 mechanosensory transduction. Cell Physiol Biochem **28,** 1051-1060.
1067 **Martinac, B., Nomura, T., Chi, G., Petrov, E., Rohde, P.R., Battle, A.R., Foo, A.,**
1068 **Constantine, M., Rothnagel, R., Carne, S., Deplazes, E., Cornell, B.,**
1069 **Cranfield, C.G., Hankamer, B., and Landsberg, M.J.** (2013). Bacterial
1070 Mechanosensitive Channels: Models for Studying Mechanosensory
1071 Transduction. Antioxid Redox Signal.
1072 **Maurel, C., Santoni, V., Luu, D.T., Wudick, M.M., and Verdoucq, L.** (2009). The
1073 cellular dynamics of plant aquaporin expression and functions. Curr Opin Plant
1074 Biol **12,** 690-698.
1075 **Mergemann, H., and Sauter, M.** (2000). Ethylene induces epidermal cell death at the
1076 site of adventitious root emergence in rice. Plant Physiol **124,** 609-614.

1077 **Miller, S., Edwards, M.D., Ozdemir, C., and Booth, I.R.** (2003a). The closed structure
1078 of the MscS mechanosensitive channel. Cross-linking of single cysteine mutants.
1079 J Biol Chem **278,** 32246-32250.
1080 **Miller, S., Bartlett, W., Chandrasekaran, S., Simpson, S., Edwards, M., and Booth,**
1081 **I.R.** (2003b). Domain organization of the MscS mechanosensitive channel of
1082 Escherichia coli. EMBO J **22,** 36-46.
1083 **Mittler, R., Vanderauwera, S., Gollery, M., and Van Breusegem, F.** (2004). Reactive
1084 oxygen gene network of plants. Trends Plant Sci **9,** 490-498.
1085 **Mousavi, S.A., Chauvin, A., Pascaud, F., Kellenberger, S., and Farmer, E.E.** (2013).
1086 GLUTAMATE RECEPTOR-LIKE genes mediate leaf-to-leaf wound signalling.
1087 Nature **500,** 422-426.
1088 **Naismith, J.H., and Booth, I.R.** (2012). Bacterial mechanosensitive channels--MscS:
1089 evolution's solution to creating sensitivity in function. Annu Rev Biophys **41,** 157-
1090 177.
1091 **Nakagami, H., Sugiyama, N., Mochida, K., Daudi, A., Yoshida, Y., Toyoda, T.,**
1092 **Tomita, M., Ishihama, Y., and Shirasu, K.** (2010). Large-scale comparative
1093 phosphoproteomics identifies conserved phosphorylation sites in plants. Plant
1094 Physiol **153,** 1161-1174.
1095 **Nakayama, Y., Yoshimura, K., and Iida, H.** (2012). Organellar mechanosensitive
1096 channels in fission yeast regulate the hypo-osmotic shock response. Nat
1097 Commun **3,** 1020.
1098 **Nakayama, Y., Fujiu, K., Sokabe, M., and Yoshimura, K.** (2007). Molecular and
1099 electrophysiological characterization of a mechanosensitive channel expressed

1100 in the chloroplasts of Chlamydomonas. Proc Natl Acad Sci U S A **104,** 5883-
1101 5888.
1102 **Nelson, B.K., Cai, X., and Nebenführ, A.** (2007). A multicolored set of in vivo organelle
1103 markers for co-localization studies in Arabidopsis and other plants. The Plant
1104 Journal **51,** 1126-1136.
1105 **Nomura, T., Sokabe, M., and Yoshimura, K.** (2008). Interaction between the
1106 cytoplasmic and transmembrane domains of the mechanosensitive channel
1107 MscS. Biophys J **94,** 1638-1645.
1108 **Nühse, T.S., Stensballe, A., Jensen, O.N., and Peck, S.C.** (2004).
1109 Phosphoproteomics of the Arabidopsis plasma membrane and a new
1110 phosphorylation site database. Plant Cell **16,** 2394-2405.
1111 **Obrdlik, P., El-Bakkoury, M., Hamacher, T., Cappellaro, C., Vilarino, C., Fleischer,**
1112 **C., Ellerbrok, H., Kamuzinzi, R., Ledent, V., Blaudez, D., Sanders, D.,**
1113 **Revuelta, J.L., Boles, E., Andre, B., and Frommer, W.B.** (2004). K+ channel
1114 interactions detected by a genetic system optimized for systematic studies of
1115 membrane protein interactions. Proc Natl Acad Sci U S A **101,** 12242-12247.
1116 **Odell, J.T., Nagy, F., and Chua, N.H.** (1985). Identification of DNA sequences required
1117 for activity of the cauliflower mosaic virus 35S promoter. Nature **313,** 810-812.
1118 **Oecking, C., and Jaspert, N.** (2009). Plant 14-3-3 proteins catch up with their
1119 mammalian orthologs. Curr Opin Plant Biol **12,** 760-765.
1120 **Okada, Y., Maeno, E., Shimizu, T., Dezaki, K., Wang, J., and Morishima, S.** (2001).
1121 Receptor-mediated control of regulatory volume decrease (RVD) and apoptotic
1122 volume decrease (AVD). J Physiol **532,** 3-16.

1123 **Orr, H.T.** (2012). SCA1-phosphorylation, a regulator of Ataxin-1 function and
1124 pathogenesis. Prog Neurobiol **99,** 179-185.
1125 **Palmieri, G., Cannio, R., Fiume, I., Rossi, M., and Pocsfalvi, G.** (2009). Outside the
1126 unusual cell wall of the hyperthermophilic archaeon Aeropyrum pernix K1. Mol
1127 Cell Proteomics **8,** 2570-2581.
1128 **Pivetti, C.D., Yen, M.R., Miller, S., Busch, W., Tseng, Y.H., Booth, I.R., and Saier,**
1129 **M.H., Jr.** (2003). Two families of mechanosensitive channel proteins. Microbiol
1130 Mol Biol Rev **67,** 66-85, table of contents.
1131 **Prado, K., Boursiac, Y., Tournaire-Roux, C., Monneuse, J.M., Postaire, O., Da Ines,**
1132 **O., Schaffner, A.R., Hem, S., Santoni, V., and Maurel, C.** (2013). Regulation of
1133 Arabidopsis leaf hydraulics involves light-dependent phosphorylation of
1134 aquaporins in veins. Plant Cell **25,** 1029-1039.
1135 **Prole, D.L., and Taylor, C.W.** (2013). Identification and analysis of putative
1136 homologues of mechanosensitive channels in pathogenic protozoa. PLoS One **8,**
1137 e66068.
1138 **Qiao, H., Shen, Z., Huang, S.S., Schmitz, R.J., Urich, M.A., Briggs, S.P., and Ecker,**
1139 **J.R.** (2012). Processing and subcellular trafficking of ER-tethered EIN2 control
1140 response to ethylene gas. Science **338,** 390-393.
1141 **Reape, T.J., and McCabe, P.F.** (2008). Apoptotic-like programmed cell death in plants.
1142 New Phytol **180,** 13-26.
1143 **Reiland, S., Messerli, G.I., Baerenfaller, K., Gerrits, B., Endler, A., Grossmann, J.,**
1144 **Gruissem, W., and Baginsky, S.** (2009). Large-Scale Arabidopsis

1145 Phosphoproteome Profiling Reveals Novel Chloroplast Kinase Substrates and
1146 Phosphorylation Networks. Plant Physiology **150,** 889-903.
1147 **Reiland, S., Finazzi, G., Endler, A., Willig, A., Baerenfaller, K., Grossmann, J.,**
1148 **Gerrits, B., Rutishauser, D., Gruissem, W., Rochaix, J.D., and Baginsky, S.**
1149 (2011). Comparative phosphoproteome profiling reveals a function of the STN8
1150 kinase in fine-tuning of cyclic electron flow (CEF). Proc Natl Acad Sci U S A **108,**
1151 12955-12960.
1152 **Reuter, M., Hayward, N.J., Black, S.S., Miller, S., Dryden, D.T., and Booth, I.R.**
1153 (2014). Mechanosensitive channels and bacterial cell wall integrity: does life end
1154 with a bang or a whimper? J R Soc Interface **11,** 20130850.
1155 **Rice, W.L., Zhang, Y., Chen, Y., Matsuzaki, T., Brown, D., and Lu, H.A.** (2012).
1156 Differential, phosphorylation dependent trafficking of AQP2 in LLC-PK1 cells.
1157 PLoS One **7,** e32843.
1158 **Schumann, U., Edwards, M.D., Li, C., and Booth, I.R.** (2004). The conserved
1159 carboxy-terminus of the MscS mechanosensitive channel is not essential but
1160 increases stability and activity. FEBS Lett **572,** 233-237.
1161 **Senthil-Kumar, M., and Mysore, K.S.** (2013). Nonhost resistance against bacterial
1162 pathogens: retrospectives and prospects. Annu Rev Phytopathol **51,** 407-427.
1163 **Sharma, S., Lin, W., Villamor, J.G., and Verslues, P.E.** (2013). Divergent low water
1164 potential response in Arabidopsis thaliana accessions Landsberg erecta and
1165 Shahdara. Plant Cell Environ **36,** 994-1008.

1166 **Sotomayor, M., van der Straaten, T.A., Ravaioli, U., and Schulten, K.** (2006).
1167 Electrostatic properties of the mechanosensitive channel of small conductance
1168 MscS. Biophys J **90,** 3496-3510.
1169 **Steffens, B., Kovalev, A., Gorb, S.N., and Sauter, M.** (2012). Emerging roots alter
1170 epidermal cell fate through mechanical and reactive oxygen species signaling.
1171 Plant Cell **24,** 3296-3306.
1172 **Steinbacher, S., Bass, R., Strop, P., and Rees, D.C.** (2007). Structures of the
1173 prokaryotic mechanosensitive channels MscL and MscS. Mechanosensitive Ion
1174 Channels, Part A **58,** 1-24.
1175 **Stühmer, W., and Parekh, A.** (1995). Electrophysiological Recordings from Xenopus
1176 Oocytes. In Single-Channel Recording (Springer US), pp. 341-356.
1177 **Suchyna, T.M., Markin, V.S., and Sachs, F.** (2009). Biophysics and structure of the
1178 patch and the gigaseal. Biophys J **97,** 738-747.
1179 **Sugiyama, N., Nakagami, H., Mochida, K., Daudi, A., Tomita, M., Shirasu, K., and**
1180 **Ishihama, Y.** (2008). Large-scale phosphorylation mapping reveals the extent of
1181 tyrosine phosphorylation in Arabidopsis. Mol Syst Biol **4,** 193.
1182 **Sukharev, S., and Sachs, F.** (2012). Molecular force transduction by ion channels:
1183 diversity and unifying principles. J Cell Sci **125,** 3075-3083.
1184 **Tabas, I., and Ron, D.** (2011). Integrating the mechanisms of apoptosis induced by
1185 endoplasmic reticulum stress. Nat Cell Biol **13,** 184-190.
1186 **van Doorn, W.G., and Woltering, E.J.** (2005). Many ways to exit? Cell death
1187 categories in plants. Trends Plant Sci **10,** 117-122.

1188 **Vasquez, V., Sotomayor, M., Cordero-Morales, J., Schulten, K., and Perozo, E.**
1189 (2008). A structural mechanism for MscS gating in lipid bilayers. Science **321,**
1190 1210-1214.
1191 **Veley, K.M., Marshburn, S., Clure, C.E., and Haswell, E.S.** (2012). Mechanosensitive
1192 channels protect plastids from hypoosmotic stress during normal plant growth.
1193 Curr Biol **22,** 408-413.
1194 **Vogel, J., and Somerville, S.** (2000). Isolation and characterization of powdery mildew-
1195 resistant Arabidopsis mutants. Proc Natl Acad Sci U S A **97,** 1897-1902.
1196 **Voinnet, O., Rivas, S., Mestre, P., and Baulcombe, D.** (2003). An enhanced transient
1197 expression system in plants based on suppression of gene silencing by the p19
1198 protein of tomato bushy stunt virus. Plant J **33,** 949-956.
1199 **Voolstra, O., Beck, K., Oberegelsbacher, C., Pfannstiel, J., and Huber, A.** (2010).
1200 Light-dependent phosphorylation of the drosophila transient receptor potential ion
1201 channel. J Biol Chem **285,** 14275-14284.
1202 **Waadt, R., and Kudla, J.** (2008). In Planta Visualization of Protein Interactions Using
1203 Bimolecular Fluorescence Complementation (BiFC). CSH Protoc **2008,** pdb
1204 prot4995.
1205 **Wang, W., Black, S.S., Edwards, M.D., Miller, S., Morrison, E.L., Bartlett, W., Dong,**
1206 **C., Naismith, J.H., and Booth, I.R.** (2008). The Structure of an Open Form of an
1207 E. coli Mechanosensitive Channel at 3.45 Å Resolution. Science **321,** 1179-1183.
1208 **Wang, X., Bian, Y., Cheng, K., Gu, L.F., Ye, M., Zou, H., Sun, S.S., and He, J.X.**
1209 (2013). A large-scale protein phosphorylation analysis reveals novel

1210 phosphorylation motifs and phosphoregulatory networks in Arabidopsis. J
1211 Proteomics **78,** 486-498.
1212 **Wilson, M.E., Maksaev, G., and Haswell, E.S.** (2013). MscS-like Mechanosensitive
1213 Channels in Plants and Microbes. Biochemistry **52,** 5708-5722.
1214 **Xin, X.F., and He, S.Y.** (2013). Pseudomonas syringae pv. tomato DC3000: a model
1215 pathogen for probing disease susceptibility and hormone signaling in plants.
1216 Annu Rev Phytopathol **51,** 473-498.
1217 **Yamada, T., Bhate, M.P., and Strange, K.** (2013). Regulatory phosphorylation induces
1218 extracellular conformational changes in a CLC anion channel. Biophys J **104,**
1219 1893-1904.
1220 **Yan, Z., Zhang, W., He, Y., Gorczyca, D., Xiang, Y., Cheng, L.E., Meltzer, S., Jan,**
1221 **L.Y., and Jan, Y.N.** (2013). Drosophila NOMPC is a mechanotransduction
1222 channel subunit for gentle-touch sensation. Nature **493,** 221-225.
1223 **Yang, X.C., and Sachs, F.** (1990). Characterization of stretch-activated ion channels in
1224 Xenopus oocytes. J Physiol **431,** 103-122.
1225 **Zhang, X., Wang, J., Feng, Y., Ge, J., Li, W., Sun, W., Iscla, I., Yu, J., Blount, P., Li,**
1226 **Y., and Yang, M.** (2012). Structure and molecular mechanism of an anion-
1227 selective mechanosensitive channel of small conductance. Proc Natl Acad Sci U
1228 S A **109,** 18180-18185.
1229
1230

A

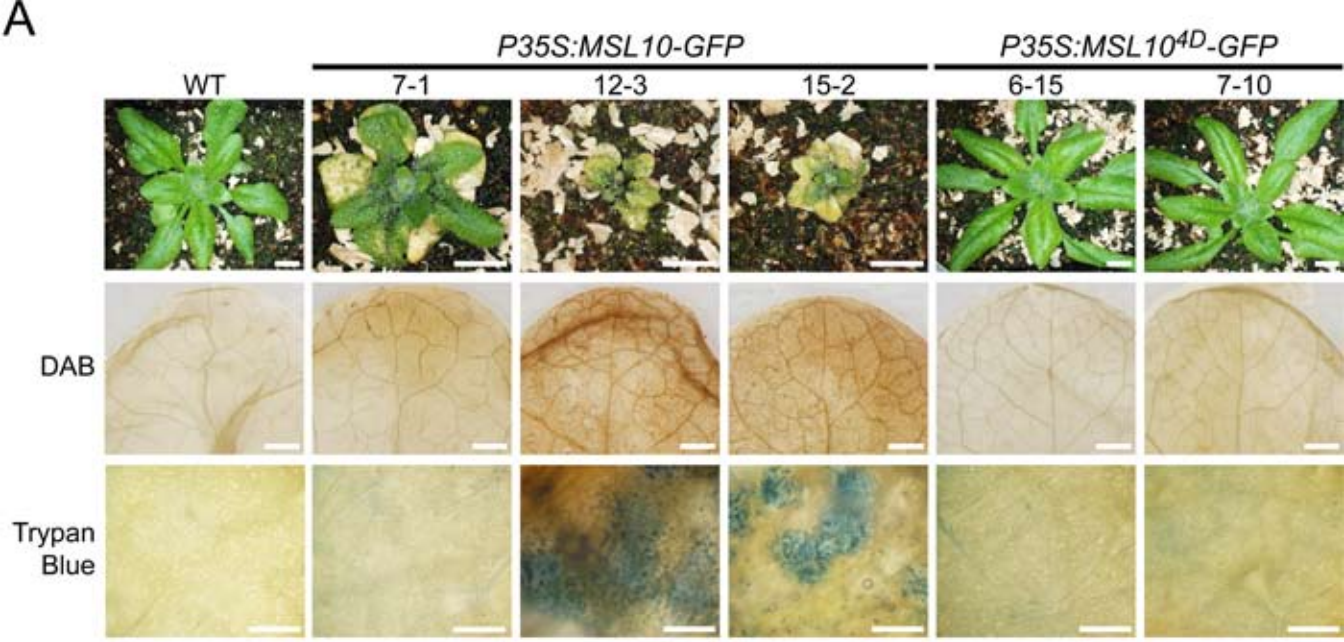
P35S:MSL10-GFP
P35S:MSL10^4D-GFP
WT
7-1
12-3
15-2
6-15
7-10
DAB
Trypan Blue

B

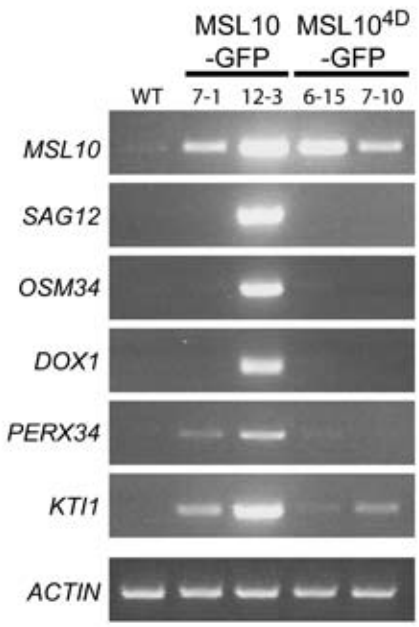
MSL10 -GFP
MSL10^4D -GFP
WT
7-1
12-3
6-15
7-10
MSL10
SAG12
OSM34
DOX1
PERX34
KTI1
ACTIN

C

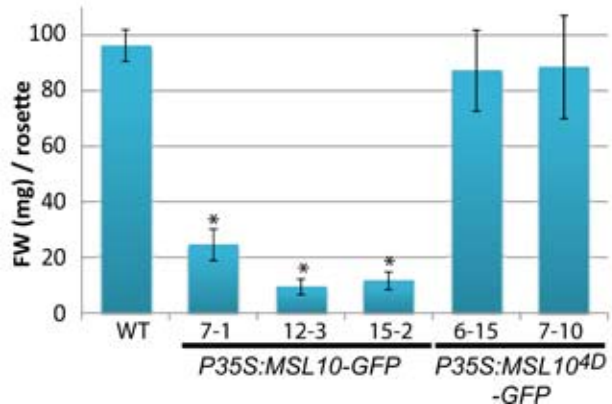
FW (mg) / rosette
100
80
60
40
20
0
WT
7-1
12-3
15-2
6-15
7-10
P35S:MSL10-GFP
P35S:MSL10^4D -GFP

D

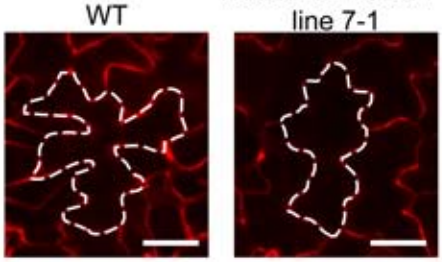
WT
P35S:MSL10-GFP line 7-1

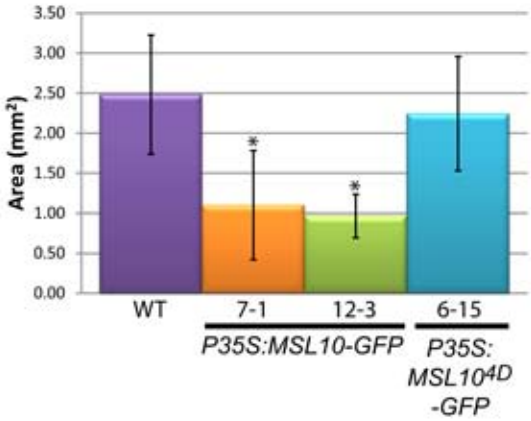
Area (mm²)
3.50
3.00
2.50
2.00
1.50
1.00
0.50
0.00
WT
7-1
12-3
6-15
P35S:MSL10-GFP
P35S: MSL10^4D -GFP

E

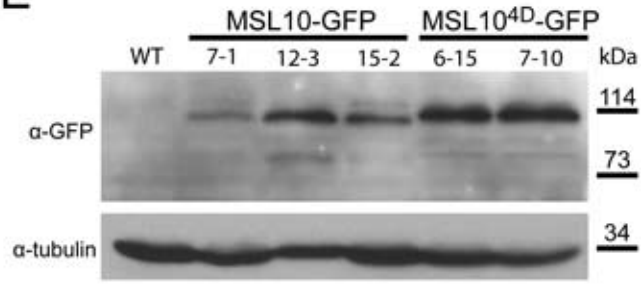
MSL10-GFP
MSL10^4D-GFP
WT
7-1
12-3
15-2
6-15
7-10
kDa
α-GFP
α-tubulin
114
73
34

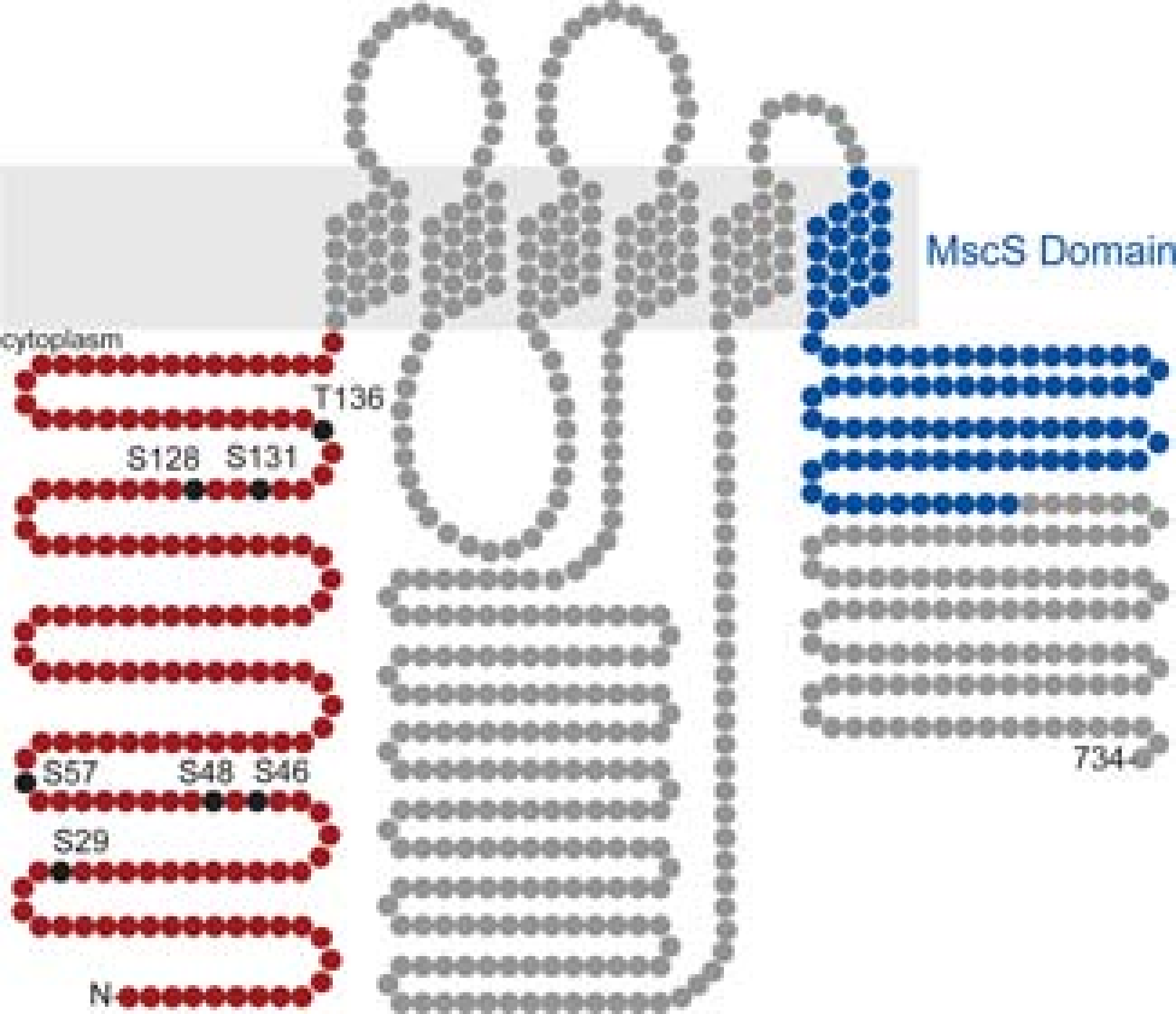
MscS Domain
cytoplasm
T136
S128
S131
S57
S48
S46
S29
N
734

A

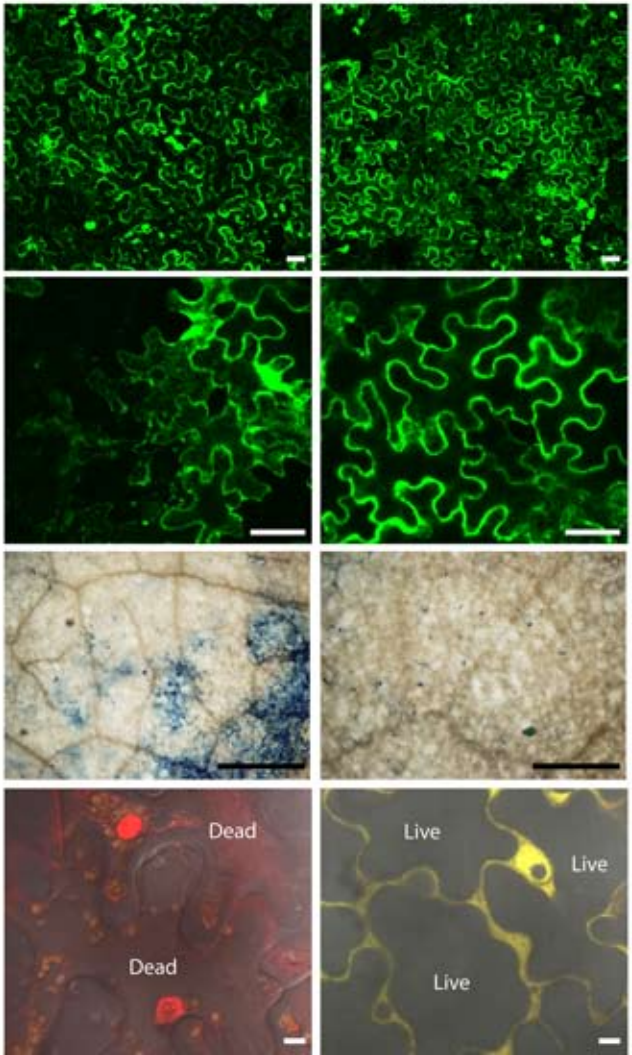
P35S:MSL10^7A-GFP
P35S:MSL10^7D-GFP
Dead
Dead
Live
Live
Live

B

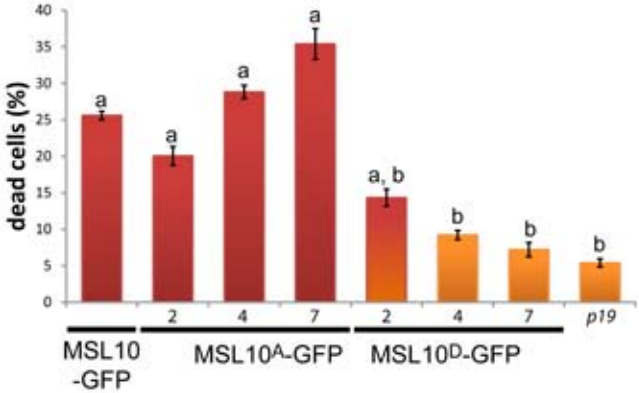
dead cells (%)
40
35
30
25
20
15
10
5
0
a
a
a
a
a, b
b
b
b
2
4
7
2
4
7
p19
MSL10 -GFP
MSL10A-GFP
MSL10D-GFP

C

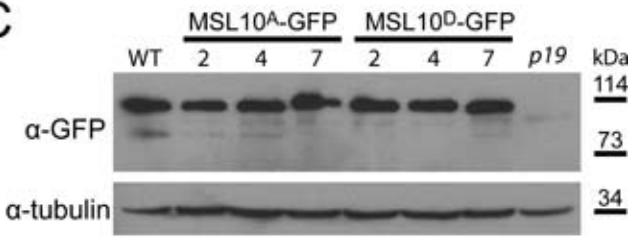
MSL10A-GFP
MSL10D-GFP
WT
2
4
7
2
4
7
p19
kDa
114
73
34
α-GFP
α-tubulin

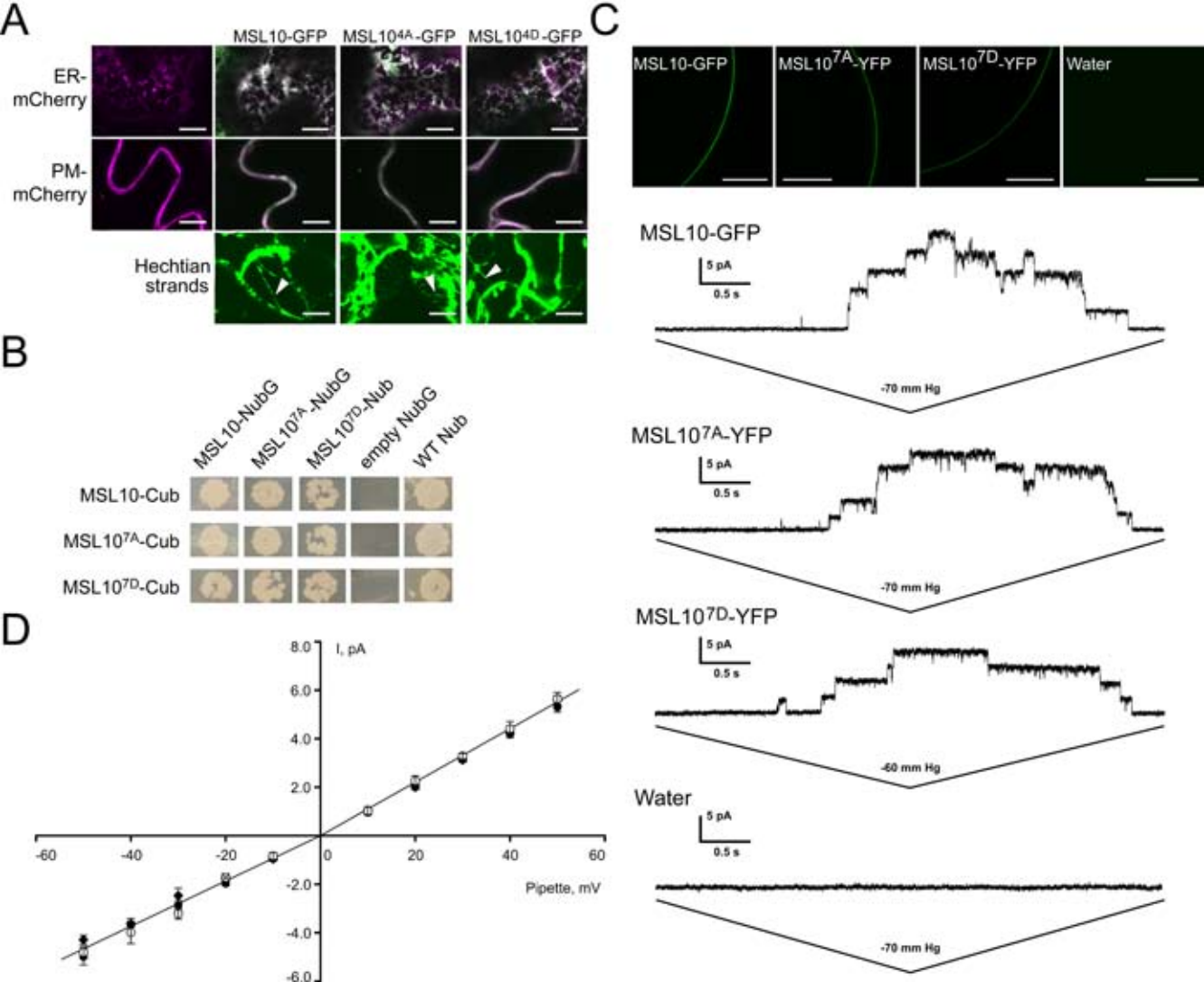
A
MSL10-GFP
MSL10^4A-GFP
MSL10^4D-GFP
ER-mCherry
PM-mCherry
Hechtian strands
B
MSL10-NubG
MSL10^7A-NubG
MSL10^7D-Nub
empty NubG
WT Nub
MSL10-Cub
MSL10^7A-Cub
MSL10^7D-Cub
C
MSL10-GFP
MSL10^7A-YFP
MSL10^7D-YFP
Water
5 pA
0.5 s
-70 mm Hg
-60 mm Hg
D
I, pA
Pipette, mV
8.0
6.0
4.0
2.0
-2.0
-4.0
-6.0
-60
-40
-20
0
20
40
60

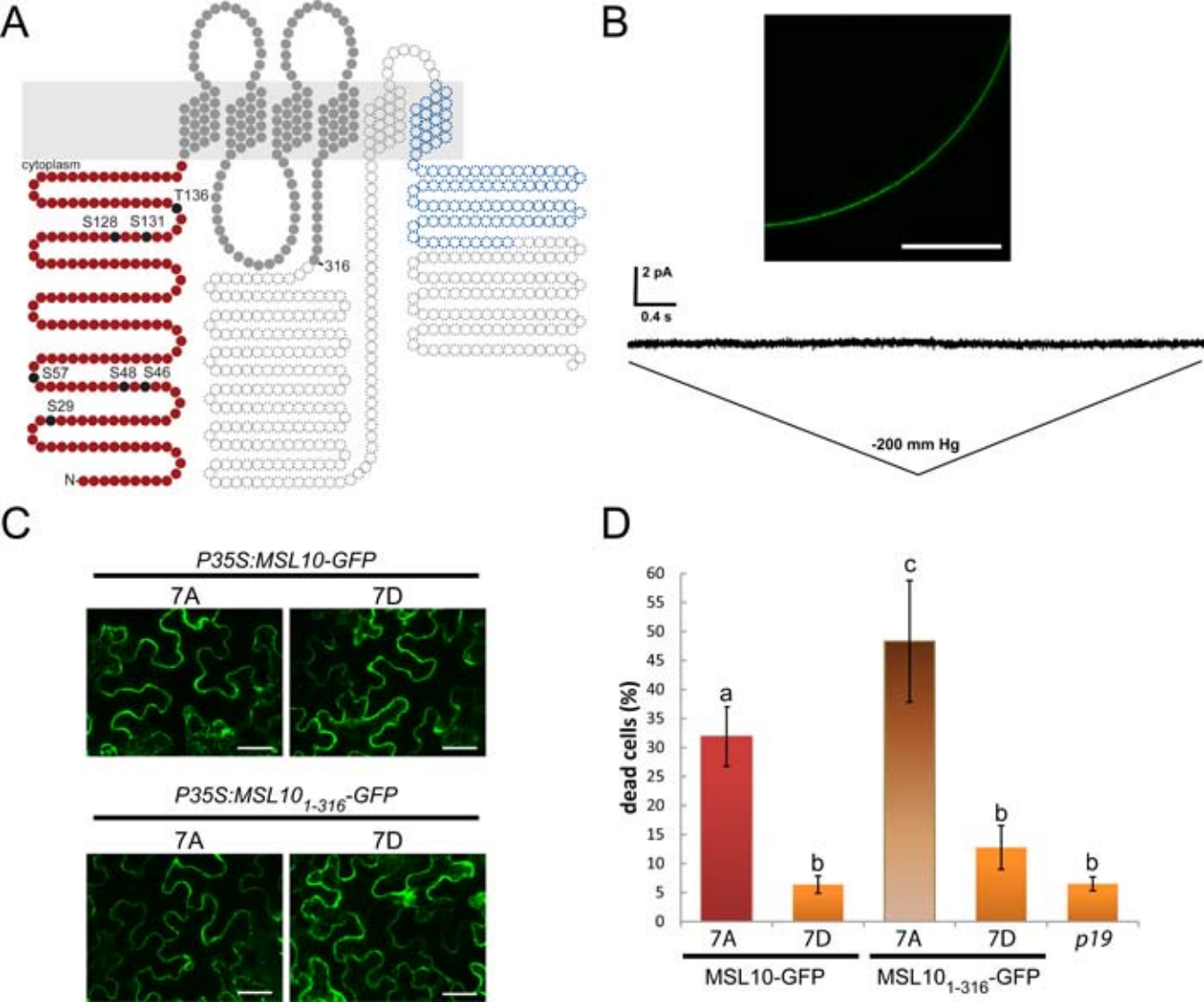
A
cytoplasm
T136
S128
S131
316
S57
S48
S46
S29
N
B
2 pA
0.4 s
-200 mm Hg
C
P35S:MSL10-GFP
7A
7D
P35S:MSL10$_{1-316}$-GFP
7A
7D
D
dead cells (%)
60
55
50
45
40
35
30
25
20
15
10
5
0
a
b
c
b
b
7A
7D
7A
7D
p19
MSL10-GFP
MSL10$_{1-316}$-GFP

A

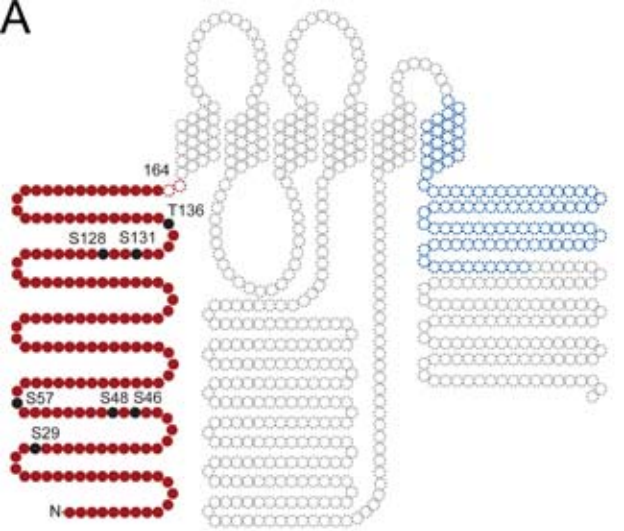
164
T136
S128
S131
S57
S48
S46
S29
N

B

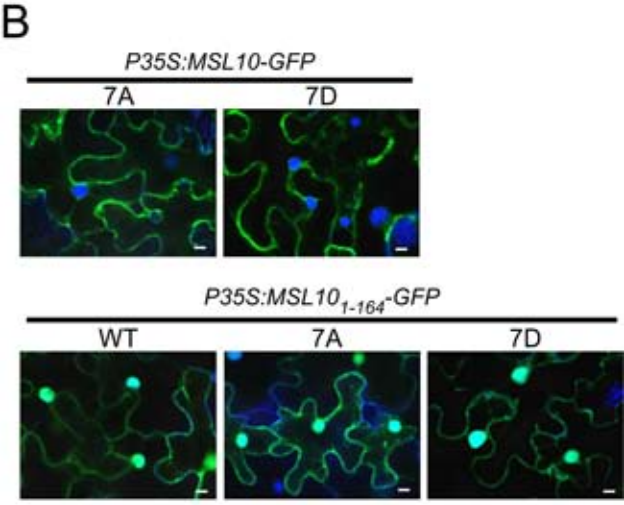
P35S:MSL10-GFP
7A
7D
P35S:MSL10$_{1-164}$-GFP
WT
7A
7D

C

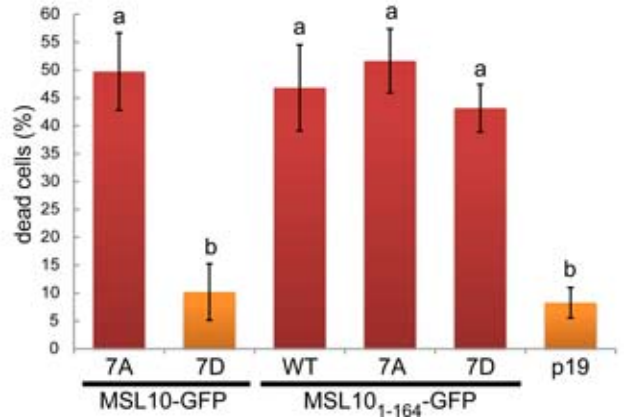
dead cells (%)
60
55
50
45
40
35
30
25
20
15
10
5
0
a
b
a
a
a
b
7A
7D
WT
7A
7D
p19
MSL10-GFP
MSL10$_{1-164}$-GFP

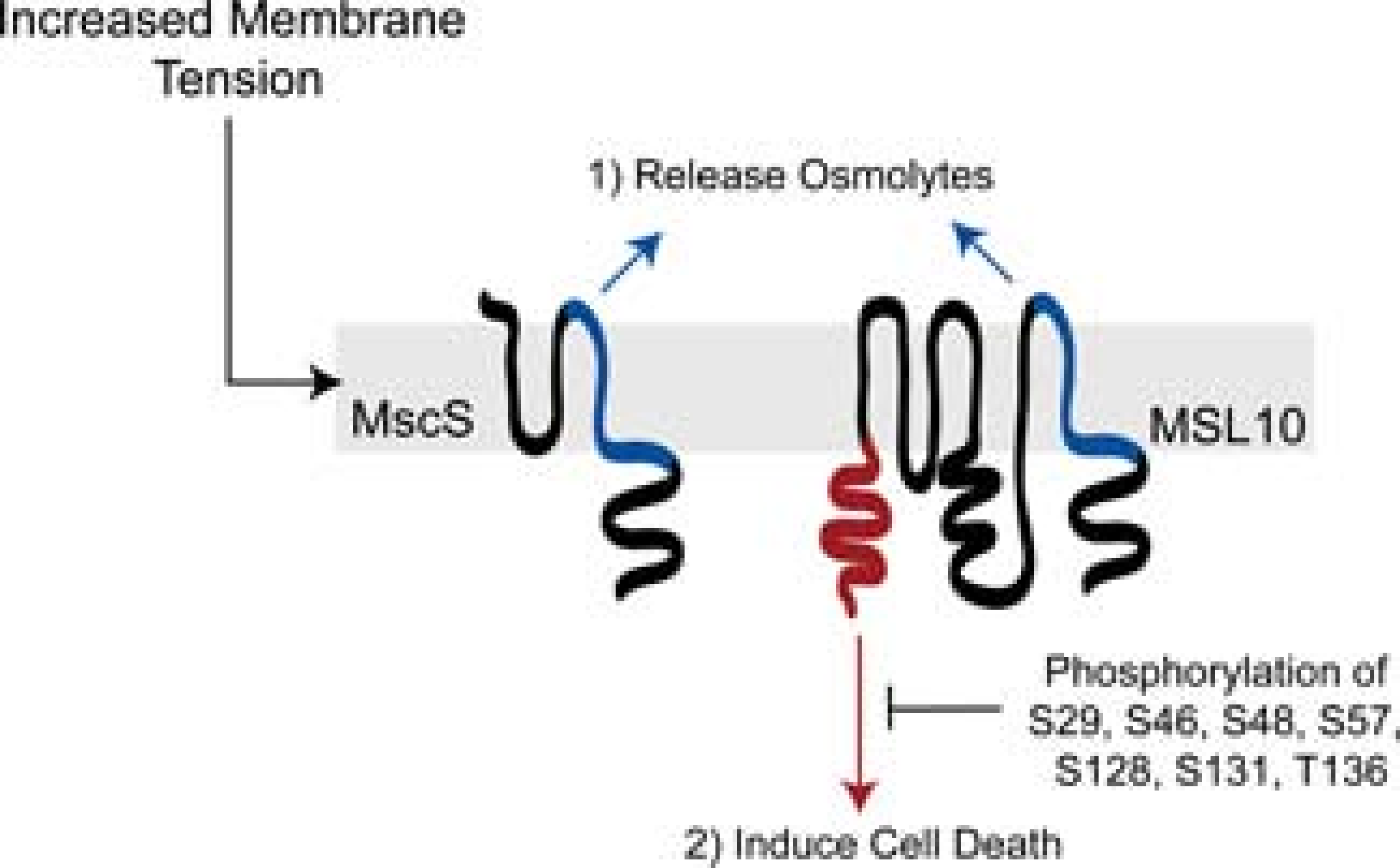
Increased Membrane Tension
1) Release Osmolytes
MscS
MSL10
Phosphorylation of S29, S46, S48, S57, S128, S131, T136
2) Induce Cell Death

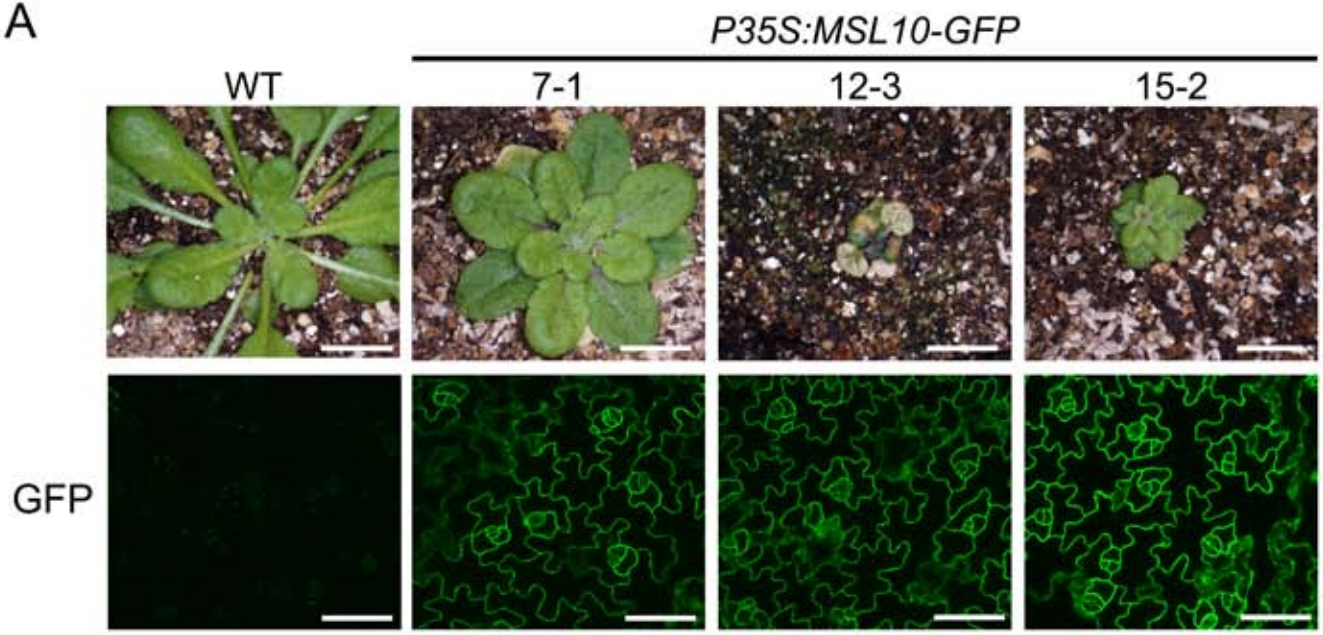

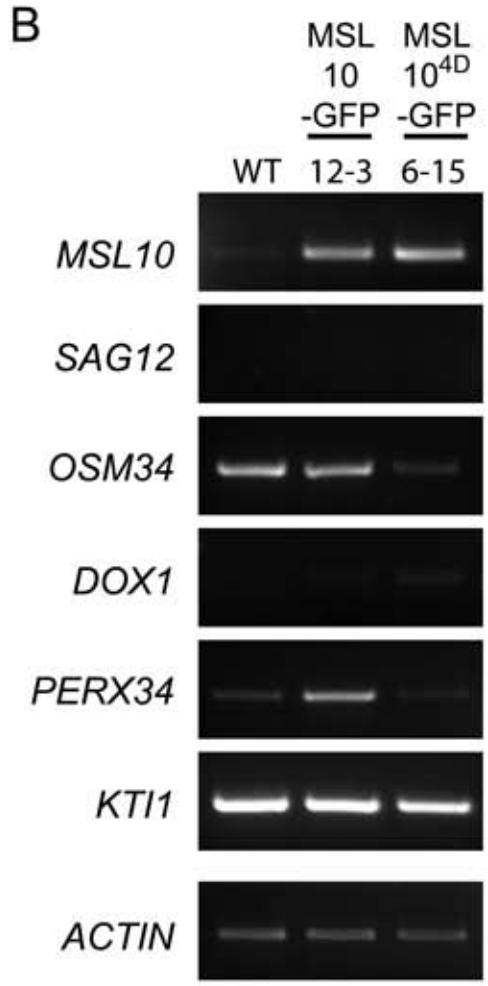

Supplemental Figure 1. Additional phenotypes associated with MSL10-GFP overexpression.

(A) Images of whole plants (top row) and of GFP signal in epidermal cells (bottom row, pseudocolored green) from four-week-old WT or homozygous transgenic T2 lines overexpressing MSL10-GFP. Plants were grown at 21°C under short day (8 hours of light) conditions. Top row: Bar = 1 cm. Bottom row: Bar = 50 µm. (B) RT-PCR analysis of cell death and ROS-related genes in WT and MSL10-GFP overexpression lines. cDNA was synthesized from RNA extracted from rosette tissue of 5-day-old seedlings grown on solid media. *ACTIN* was used as a control.

```
MSL10                  1 ---------------MAEQKSSNGGGG-------GGDVVINVPV----EEASRRSKEMASPESEKGVPFS--------
Populus trichocarpa    1 -----------MEAGKGVIDKKGTNDVVIHISTTNQDATTKAYSFSKNSQLGSSPKDSSSNLELTEFENLS-------
Cucumis sativus        1 ------------MDVSGNKGIRRGSSQKESG--NGGEVVVQLSG---VENECSVPKQNRADSQTKEPTGS--------
Vitis vinifera         1 ---------------MSEKKETGGAEVVVTISAESKEANANTKGSSPMDSETSAPRRSGQGVTEAKTQPH--------
Medicago truncatula    1 ----------------MEKK----TEVVVAISNVGGDTHHHG--QDHDHELKGVES--SPRYSTKSPPLN--------
Theobroma cacao        1 ------------MEANKDTAEKRGTGGEVVINVSGEDTLKGPKGSAPKEAEALAAKQSAQDAADKASTESGAVTTGLA
Ricinus communis       1 ---------------MAEKKTSNGGRGEVLITISGDETPKGSAS---KDSDSVASKQSRPSSPVKESNGG-----AFA
Arabidopsis lyrata     1 ---------------MAEQKSSNGGG---------GEVVINVSG----EEASKRSMEMASPESEKGVPIS--------
Citrus clementina      1 MDAEEKAAVKGGEISMSEKKNVNGSEVVIKISSDESPKDNVDARNSKGSSSEATTEPVTAGFAAKSVPAS--------
Solanum lycopersicum   1 ------------MDANGKAVKFSGEIGMAENKKPPSDVVVMISGDERDSNSPVRPPRSTVDPPIVSQIPR--------
Glycine max            1 ------MVLKGGEVSMSEKK----REVMVAIPHEGGAESLMPKQQSRVNSPHRALN--DNEVAAKSPPLN--------

MSL10                 45 ---KSPSPEISKLVGSP----NKPPRAPNQN-NVGLTQRKSFARSVYSKPKSRFVDPSCPVDTSILEEE--VR--EQL
Populus trichocarpa   62 RVQTSPSSEIPKPSPAPSPTPHKPPKIPTT---DSITRRKSLARSEFSKPKSRLVEPSYPYDAILKEEMKTGQ----S
Cucumis sativus       54 -SVGYDN--ASPLAPTP----NKPPKIPIS--NGTLTPRRSLRRSTLSKPKSRFGEQSCFIDSDMLEEENHVS--LRE
Vitis vinifera        56 ----CPSPEIAGFTGSP----HKPPKIPTS---EALARRRSVAKSVYSRSKSRFG--DPPVDINYFENNNGIL--QEQ
Medicago truncatula   47 ----CASP-EIRFIPSP----NKPPKVPATN--ESLTPRKTLVRSVFSKPKSRFGEQPYPIDGTLLEENVTSSNLQDQ
Theobroma cacao       69 VPVGCPSPETSKFGPTT----NKPPKVPSPG-NESFTRRRSFARSLNSKPKSRFGEQSYVLESDQTEENGLVN--REQ
Ricinus communis      58 VSINNHSPEISSLNPTP----TKPPKIPVS--NENLTRRRSLARSVYSKPKSRFGEQPVLVDATVLEEDSLIL--EEQ
Arabidopsis lyrata    43 ---KSPSPEISKLVGSP----NKPPRAPNRN-NEGLTQRKSFARSVYSKPKSRFVDPSCPVDTTVLEEE--VR--EQL
Citrus clementina     71 ----SPSP-EIRFASSP----NKPPKIPTTNEAATLARRRSLARSVYSKPKSRFGEPSY-IDDNAFDEHVDLS-RRDQ
Solanum lycopersicum  60 VQVNDSSPEISRYTPTPSPSANKPPKIPTN---ETLSRRKSFASSAFSKPKSRFGEQSLPIDANMFDEQPEPS--ANS
Glycine max           59 ----CASP-EIRFMPSP----NKPPKVPTSN--AILTRRKSLTRSVYSKPKSRFGEQSYPIDGTLLEENATST-LQEN

MSL10                113 GFSFSRASPNNKS--------NRSVGSPA-------PVTPSKVVVE-KDEDEEIYKKVKLNREMR---SKI
Populus trichocarpa  135 SSSPRNVASPNDTLGVTTPRDNLRSAPIT-------PKTPLIGTPGLDDDDDEVYRTAILNLGKITG-KKW
Cucumis sativus      123 GATSSRSSN-------------LNTPKAQ-------PEGEDDGNMG-SN-------------AKH---KKV
Vitis vinifera       121 GSSSYRSYRASPG-----SKPGSRAVSIN----QRTPLMASPGGVE-DD-DEEIYKRVNSTEWNKKKHRRV
Medicago truncatula  116 VTSPYKASRS----PNNKHGTVYRTVSITSVVTPRTPLMTSPGPAG-EDPDEIIYKKVEFSKGKR---KRL
Theobroma cacao      142 GNSPYRHSFNKAS-PNNKSARSIRTDSAV-------SKTLSIGTTG-ENEYEEIIKKVKLHKEKL---KGV
Ricinus communis     130 RNLSYRKSLSRGS-ANNKSASSIRTNSMN-------PNGPVDD----EDEVEDVVKKVQSIKEKN---KRV
Arabidopsis lyrata   111 GFSFSRSSPNNKS--------NRSVGSTA-------PLTPSKAVVE-KDEDEEIYKKVKLNKEMR---SKI
Citrus clementina    140 VNSPYRTSFSRAS-PNSKSGLSARTNSIT----PKTPLMASPRGPG-ED-DEEIYKKVKLIKEQR---NKV
Solanum lycopersicum 135 RNVSNRASPTAKMGSTDTFKETTRTVSIS--VTPRTPLMASPGGFGGVDEDEEIYKKVSSRKKLKY--NKF
Glycine max          127 VGSPYKASPN----NNNKPGTVNRTFSILSVVTPKTPLMASPGLAG-EDFDEIIYKKVELSKNMRS--RRL
```

Supplemental Figure 2. Multiple sequence alignment of the N-termini of MSL10-like orthologs in land plants.

Protein sequence alignment of MSL10 and its putative orthologs from other plant species. Sequences used in the alignment were defined by the predicted MSL10 cytoplasmic N-terminus (aa 1-164). MSL10 and the species names from which putative orthologs were found are noted to the left of the sequences. The alignment was made using ClustalX (Larkin et al., 2007). Dark shading of residues within the sequences indicates at least 50% identity and light grey shading indicates at least 50% similarity.

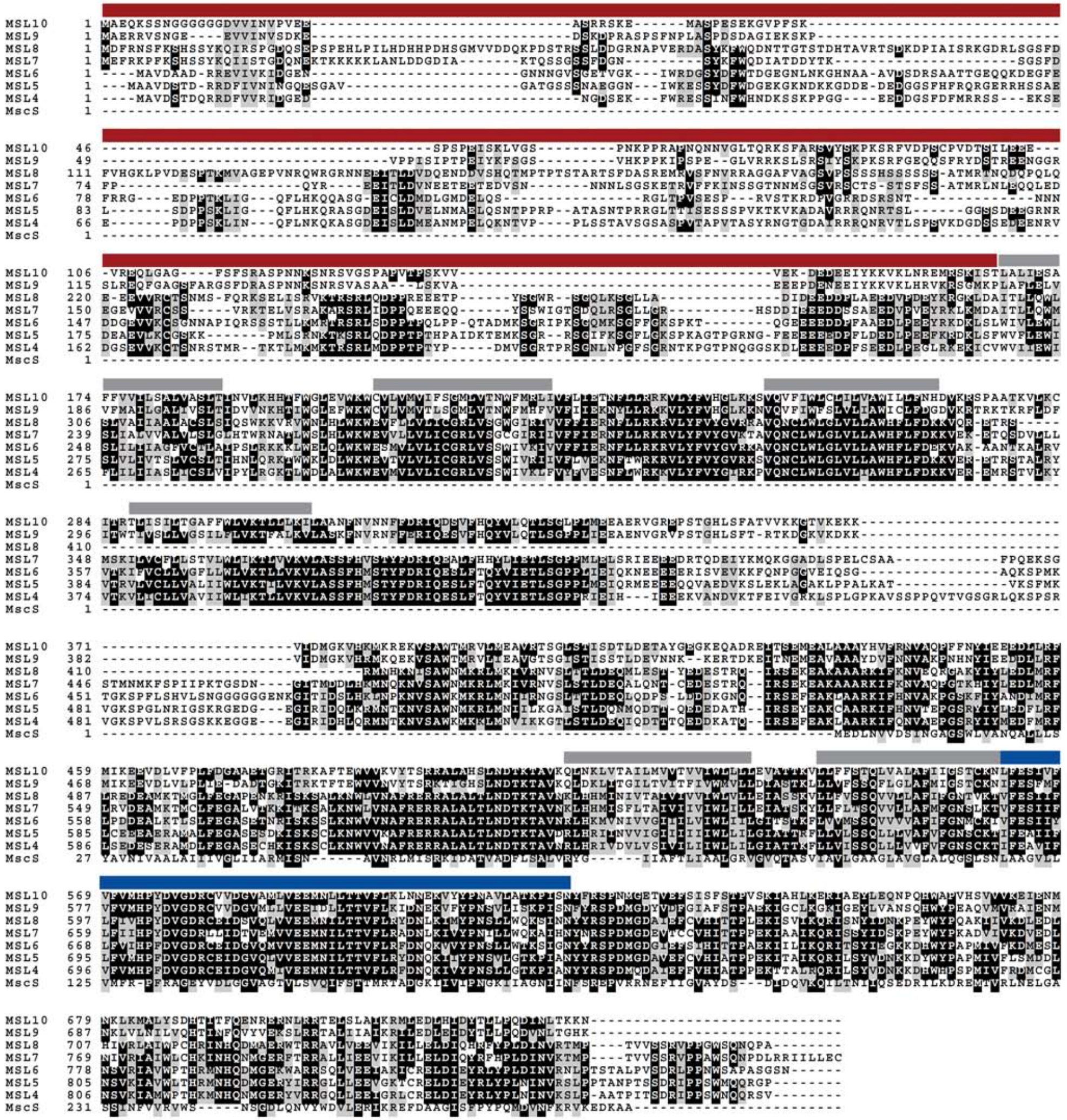

Supplemental Figure 3. Multiple sequence alignment of Class II MSL proteins from *Arabidopsis thaliana* and MscS from *Escherichia coli*.

The colored boxes above the sequences coordinate with the colors used to indicate the relevant domains of MSL10 in Figure 2. The predicted cytoplasmic N-terminal region is indicated in brick red, TM helices are grey, and the region of highest homology with MscS is dark blue. Note the low level of conservation in the red-highlighted region. The alignment was made using ClustalX (Larkin et al., 2007). Dark grey shading of residues indicates at least 50% identity across sequences and light grey shading indicates at least 50% similarity.

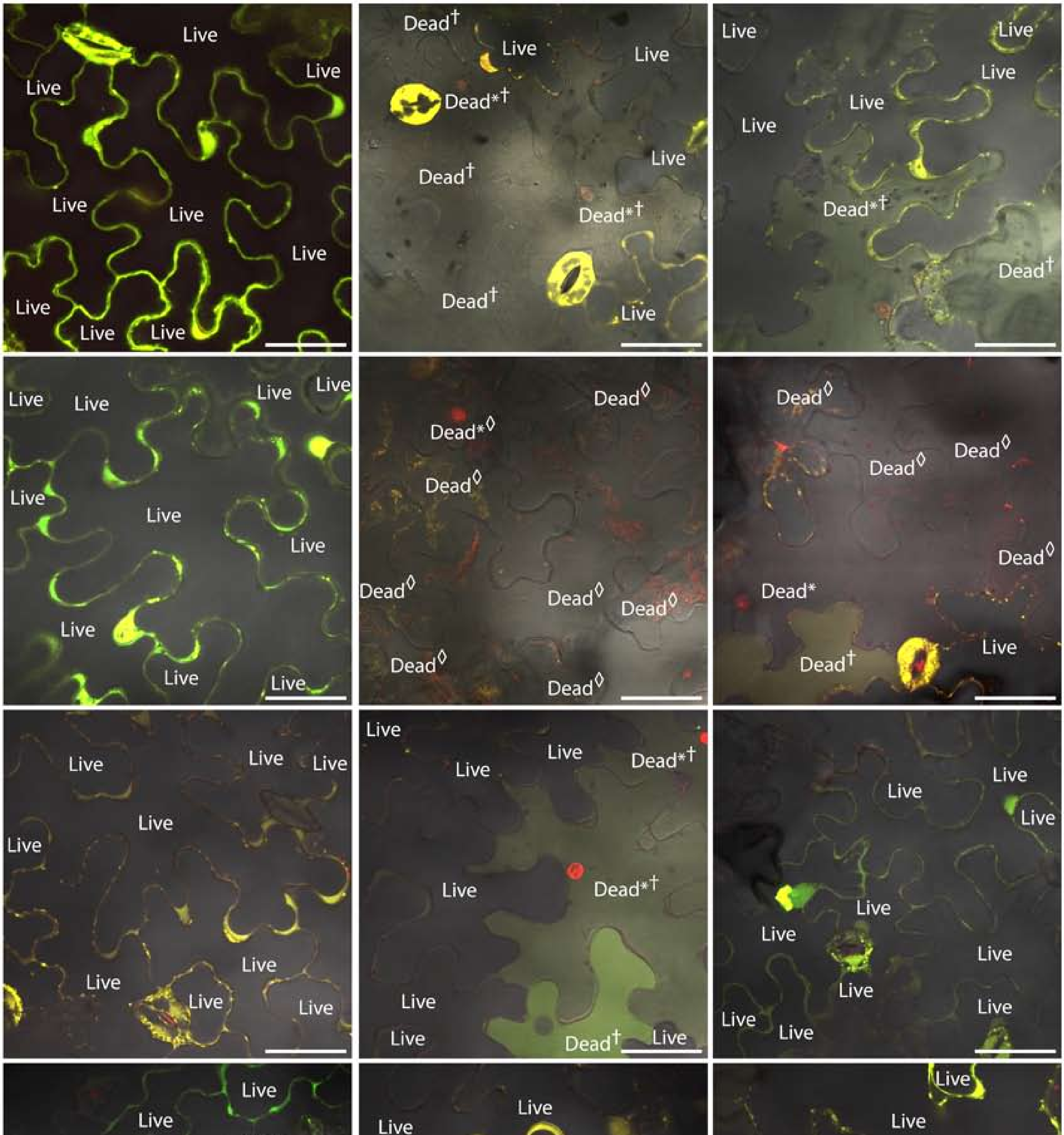

Supplemental Figure 4. Documentation of the cell death assay used in Figures 3, 5, and 6.

Representative CLSM images used to quantify cell death in tobacco leaves 5 days after infiltration with Agrobacterium harboring the indicated MSL10-GFP variant and the expression enhancer p19. Epidermal cells from the abaxial side of the infiltrated tobacco leaf epidermis were imaged 5 days post-infiltration for the analysis. Fluorescein diacetate (FDA, pseudocolored green) and propidium iodide (PI, pseudocolored red) staining was used to aid in the determinaltion of whether a cell was “dead” or “live”. Cells were classified as “live” unless they fulfilled one or more of the following criteria: 1) the presence of PI signal in the nucleus (*), 2) other PI-staining particles or compartments in the cell center (◊), and/or 3) the disappearance of an obvious vacuole, accompanied by spreading of cytoplasmic GFP/FDA signal (†). Bar = 50 µm.

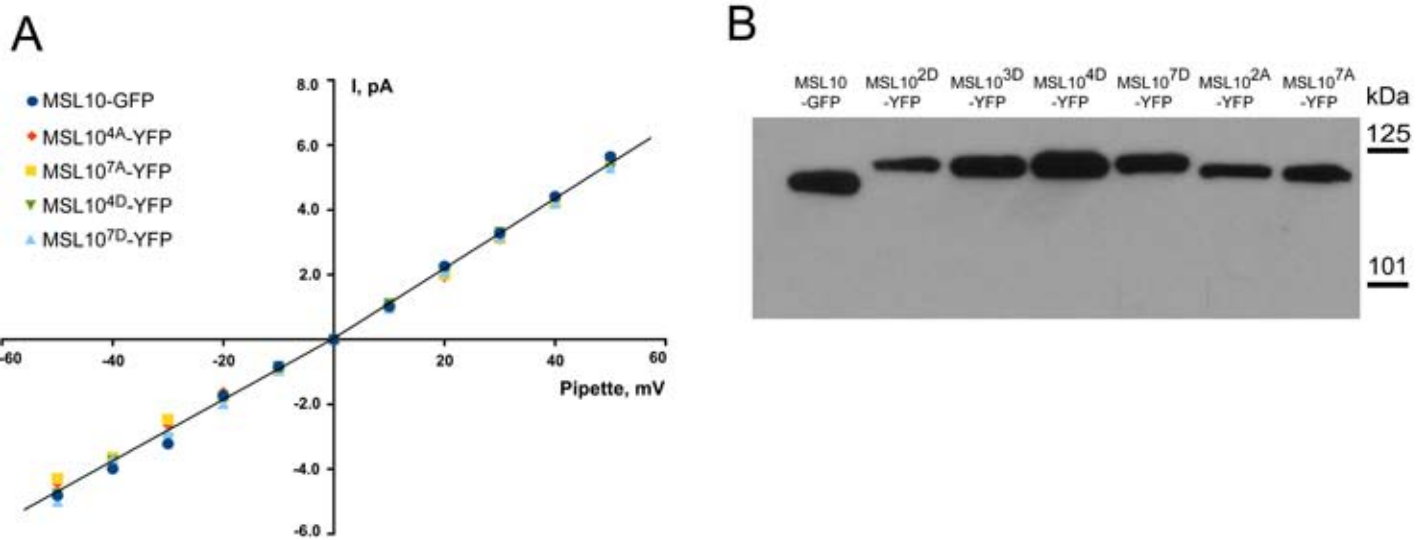

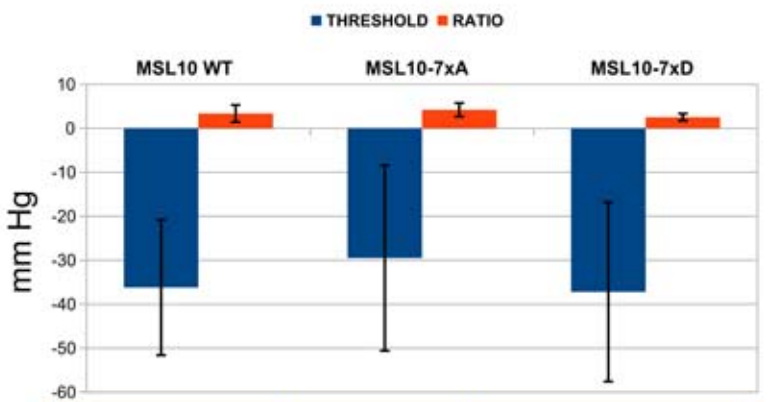

	Gating threshold, mm Hg	Open/close pressure ratio	Statistics
MSL10 WT	-36.2 ± 15.4	3.38 ± 1.94	22/20 traces, 10 oocytes
MSL10 7xA	-29.5 ± 21.1	4.21 ± 1.55	6/5 traces, 5 oocytes
MSL10 7xD	-37.2 ± 20.4	2.54 ± 0.81	6/5 traces, 5 oocytes

Supplemental Figure 5. Electrophysiological analysis of MSL10 variants in Xenopus oocytes.

(A) Current/voltage curves for MSL10 variants under membrane tension in symmetric modified ND96 buffer 7 days post-injection (n = 3 oocytes for each protein). The GFP/YFP tag did not affect MSL10 ion channel properties (Maksaev and Haswell, 2012). (B) Immunoblot on isolated membrane extracts from Xenopus oocytes 7 days post-injection. The equivalent of 1 oocyte was used for immunoblot analysis for each sample. Blot was detected with an anti-GFP primary antibody to detect MSL10-GFP or –YFP. Protein sizes are indicated at the right according to a commercially available standard. (C) Quantification of gating thresholds and open/close pressure ratios for MSL10 variants expressed in oocytes. Sample sizes are indicated in the figure table and error bars indicate standard deviation.

Supplemental Table 1. Experimentally determined *in vivo* phosphorylated peptides attributed to MSL10.

Residue	Sequence	Experimentally tested conditions *in vivo*
S29	(pS)KEMASPESEK	Seedlings upon resupply of nitrogen after starvation (Engelsberger and Schulze, 2012)
S46	GVPFSK(pS)PSPEISK	Suspension cell cultures derived from stem explants (Sugiyama et al., 2008; Nakagami et al., 2010)
S48	GVPFSKSP(pS)PEISK	Suspension cell cultures derived from stem explants (Sugiyama et al., 2008; Nakagami et al., 2010)
S57	LVG(pS)PNKPPR	Suspension cell cultures derived from stem explants (Nühse et al., 2004), mesophyll suspension cell culture (Benschop et al., 2007), whole shoots from 22-day-old soil-grown plants (Reiland et al., 2009), ethylene-treated etiolated *ein2* seedlings (Li et al., 2009), 9-day-old seedlings (Wang et al., 2013)
S128	(pS)VGSPAPVTPSK	Suspension cell cultures derived from stem explants (Nühse et al., 2004), mesophyll suspension cell culture with and without flg22 treatment (Benschop et al., 2007), 6-week-old plants (Reiland et al., 2011), 9-day-old seedlings (Wang et al., 2013)
S131	SVG(pS)PAPVTPSK	Whole shoots from 22-day-old soil-grown plants (Reiland et al., 2009), mesophyll suspension cell culture with and without xylanase treatment (Benschop et al., 2007)
T136	SVGSPAPV(pT)PSK	Suspension cell cultures derived from stem explants (Nühse et al., 2004), mesophyll suspension cell culture (Benschop et al., 2007)

Supplemental Table 2. Primers used for Reverse-Transcription Polymerase Chain Reaction experiments.

Primer name	Sequence	# cycles used
12080.F1 12080.R1	ATGGCAGAACAAAAGAGTAGTAACG CTTACTGCGCATCTCTCTGTTCAG	27
PERX34_F1 PERX34_R1	CAACATCGTCCACTTGGACAATCTT CCTGCCAAAGTGACAGATTGTTGAG	30
DOX1_F1 DOX1_R1	ATCGGTTTCTTCTTCTTATCGTG TTTGATTTCTGATCGACGGGG	30
SAG12_F1 SAG12_R1	CCACTCGACAATGAACTCAT TGACTCAGTTGTCAAGCC	35
ATKTI1_F1 ATKTI1_R1	CCCGAATCACAGAACCTCAA GAACATAACCAAGAACGGCTTATC	30
OSM34_F1 OSM34_R1	CTGAGTACGCTTTGAACCAATTC TCTCCTCGGTGACCATCTT	30
ACT.F2 Actin.8	TACGCCAGTGGTCGTACAAC AACGACCTTAATCTTCATGCTGC	25

Supplemental References

Benschop, J.J., Mohammed, S., O'Flaherty, M., Heck, A.J., Slijper, M., and Menke, F.L. (2007). Quantitative phosphoproteomics of early elicitor signaling in Arabidopsis. Mol Cell Proteomics **6,** 1198-1214.

Dixit, R., Rizzo, C., Nasrallah, M., and Nasrallah, J. (2001). The brassica MIP-MOD gene encodes a functional water channel that is expressed in the stigma epidermis. Plant Mol Biol **45,** 51-62.

Engelsberger, W.R., and Schulze, W.X. (2012). Nitrate and ammonium lead to distinct global dynamic phosphorylation patterns when resupplied to nitrogen-starved Arabidopsis seedlings. The Plant Journal **69,** 978-995.

Kabsch, W., and Sander, C. (1983). Dictionary of protein secondary structure: pattern recognition of hydrogen-bonded and geometrical features. Biopolymers **22,** 2577-2637.

Larkin, M.A., Blackshields, G., Brown, N.P., Chenna, R., McGettigan, P.A., McWilliam, H., Valentin, F., Wallace, I.M., Wilm, A., Lopez, R., Thompson, J.D., Gibson, T.J., and Higgins, D.G. (2007). Clustal W and Clustal X version 2.0. Bioinformatics **23,** 2947-2948.

Li, H., Wong, W.S., Zhu, L., Guo, H.W., Ecker, J., and Li, N. (2009). Phosphoproteomic analysis of ethylene-regulated protein phosphorylation in etiolated seedlings of Arabidopsis mutant ein2 using two-dimensional separations coupled with a hybrid quadrupole time-of-flight mass spectrometer. Proteomics **9,** 1646-1661.

Maksaev, G., and Haswell, E.S. (2012). MscS-Like10 is a stretch-activated ion channel from Arabidopsis thaliana with a preference for anions. Proc Natl Acad Sci U S A **109,** 19015-19020.

Nakagami, H., Sugiyama, N., Mochida, K., Daudi, A., Yoshida, Y., Toyoda, T., Tomita, M., Ishihama, Y., and Shirasu, K. (2010). Large-scale comparative phosphoproteomics identifies conserved phosphorylation sites in plants. Plant Physiol **153,** 1161-1174.

Nühse, T.S., Stensballe, A., Jensen, O.N., and Peck, S.C. (2004). Phosphoproteomics of the Arabidopsis plasma membrane and a new phosphorylation site database. Plant Cell **16,** 2394-2405.

Reiland, S., Messerli, G.I., Baerenfaller, K., Gerrits, B., Endler, A., Grossmann, J., Gruissem, W., and Baginsky, S. (2009). Large-Scale Arabidopsis Phosphoproteome Profiling Reveals Novel Chloroplast Kinase Substrates and Phosphorylation Networks. Plant Physiology **150,** 889-903.

Reiland, S., Finazzi, G., Endler, A., Willig, A., Baerenfaller, K., Grossmann, J., Gerrits, B., Rutishauser, D., Gruissem, W., Rochaix, J.D., and Baginsky, S. (2011). Comparative phosphoproteome profiling reveals a function of the STN8 kinase in fine-tuning of cyclic electron flow (CEF). Proc Natl Acad Sci U S A **108,** 12955-12960.

Sugiyama, N., Nakagami, H., Mochida, K., Daudi, A., Tomita, M., Shirasu, K., and Ishihama, Y. (2008). Large-scale phosphorylation mapping reveals the extent of tyrosine phosphorylation in Arabidopsis. Mol Syst Biol **4,** 193.

Wang, X., Bian, Y., Cheng, K., Gu, L.F., Ye, M., Zou, H., Sun, S.S., and He, J.X. (2013). A large-scale protein phosphorylation analysis reveals novel phosphorylation motifs and phosphoregulatory networks in Arabidopsis. J Proteomics **78,** 486-498.